Sustainable Structures
ISSN: 2789-3111 (Print); ISSN: 2789-312X (Online)
http://www.sustain-dpl.com/journal/sust
DOI: 10.54113/j.sust.2025.000078

ORIGINAL ARTICLE

Experimental study of load transfer mechanisms of onshore wind turbine foundations

Janet Modu[a, b], Laurent Briançon[a*], Jean-François Georgin[a], Eric Antoinet[b]

[a] GEOMAS, Université de Lyon, INSA-Lyon, Villeurbanne, France
[b] ANTEA GROUP, Olivet, France
[*]Corresponding Author: L. Briançon. Email: laurent.briancon@insa-lyon.fr

Abstract: In Europe, the development of the wind energy market will evolve between 2020 and 2030 towards a renewal of existing wind farms to reach the objectives set by the law on energy transition for green growth. This renewal process involves the replacement of wind turbines after their service lives by more powerful machines, which would necessitate reconstruction of new foundations to accept the loads of the larger turbine. To reduce environmental impacts and limit greenhouse gas emissions, this practice appears to be far from optimal. This paper therefore focuses on assessing the suitability of a 1g small-scale model as a tool to support an evolutionary design enabling reuse of existing foundations during repowering. As part of the FEDRE research project, the study evaluates the model's ability to simulate foundation behavior under quasi-static loading. The broader methodology integrates field monitoring, small-scale testing, and COMSOL Multiphysics® simulations to assess the feasibility of reuse before proposing practical solutions.

Keywords: Onshore wind turbines, small-scale modeling, reinforced concrete foundation, scaling laws, finite element modeling

1 Introduction

Onshore wind energy has become an important source of renewable energy in the French industry, and more widely in the European energy mix. The energy-producing structures from land-based wind, more widely termed as 'onshore wind turbines' have a lifespan of about 20 to 25 years after which the problem of renewing the park arises for the operator. During the renewal phase, now commonly known as 'repowering phase', the height of the masts would be increased to reach higher wind speeds resulting to greater wind turbine power. This generates increased forces at the base of the mast. The existing footing is therefore considered no longer adapted to the loads of the taller, more powerful newly installed superstructure. The solution currently practiced in France during full repowering is deconstruction of the existing footing and reconstruction of a heavier footing to resist the higher loads of the new superstructure. Considering this current solution, there exists a significant environmental impact in addition to the cost of reconstruction, since the production of one ton of cement necessary for the production of reinforced concrete requires the emission of about 900 kg of carbon dioxide.

As a means to overcome the limitations incorporated in the current repowering solution, the FEDRE project FUI25 (Fondations d'Eoliennes Durables et REpowering) is introduced whose primary mission is to improve the competitiveness of the industry by optimizing wind turbine foundations through reuse of existing foundations. This involves determining and proposing an evolutionary design of the foundations that would allow installation of two, or even three successive generations of wind

Received: 8 January 2025; Received in revised form: 1 May 2025; Accepted: 3 May 2025

turbines. According to [1], partial repowering has been a strategy from as recently as year 2017. A strategy that strongly depends on the integrity and capacity of the existing foundations for the long-term success of repowering efforts. This therefore requires a thorough, detailed, and comprehensive review of existing foundations, including strength, serviceability, and fatigue analyses.

The current paper therefore presents and discusses the results of an investigation conducted to simulate the load transfer mechanism of existing onshore wind turbine foundations due to the effect of wind loading. This is one amongst other loading types the wind turbine is subjected to during its lifetime.

2 Methods

To study this behavior, the methodology presented in **Fig. 1** is adopted. It involves monitoring of a real wind turbine, numerical simulations, and laboratory small-scale models. Firstly, sensor measurements of existing wind turbines are compared to numerical simulations, and it is through numerical modeling small-scale models are verified. A similar methodology relating physical and numerical models to in-situ measurements was adopted by [2] to construct a reactor containment in Paris, Frnce.

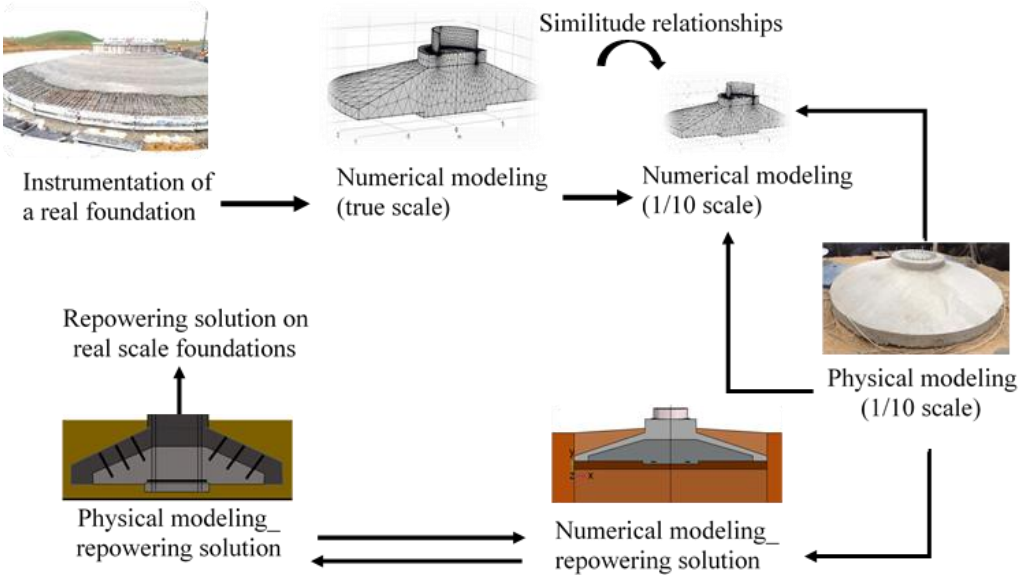

Fig. 1. Methodology adopted in the FEDRE Project.

By integrating data from monitoring a real wind turbine foundation, conducting numerical simulations, and analyzing laboratory small-scale models, it is hypothesized that the load transfer occurs through a complex interaction between the foundation structure, soil properties, and the action of wind loading. In fact, very few papers speak of 1-g small-scale modeling of multiple interactions associated with gravity-based wind turbine foundations. The paper therefore highlights the extent to which a 1/10 downscaled model remains a promising tool in simulating these interaction problems, more specifically within the elastic region. It is emphasized that since small-scale models in geomechanics are seldom exact replicas of their equivalent real structures, they should be used alongside numerical models. In addition, results from small-scale models should not be directly upscaled for the design of real-scale structures, and results interpreted with caution. Reference can be made to [3] for the use of physical models in the verification and validation of innovative design concepts, taking into account all possible angles to de-risk a project.

2.1 Loading and mechanisms occurring in onshore wind turbines

The process of understanding existing wind turbines foundations involves identification of loading mechanisms associated with them. Onshore wind turbines are typically subjected to repeated tilting forces due to wind action throughout their lives in directions that can vary by 360 °. Due to the random occurrence of the wind action both in space (spatial) and time (temporal), it is classified as variable fixed actions according to EN 1990, 4.1.1 and are therefore better described statistically. Considering

the nature of the wind load, they may impose either one-way or two-way cyclic loading. In the context of soil-structure interaction, one-way loading is known to develop more soil deformation and consequently more change in foundation stiffness [4].

In the context of an offshore wind turbine, [5] reports the wind turbine being subjected to about 10 to 100 million load cycles of varying amplitudes within its lifetime of 25 to 30 years. This causes the underlying foundation to undergo two superimposed loading conditions: 1) Cyclic overturning moments due to wind loading (typical frequency of 0.01 Hz) and 2) Dynamic effects such as resonance. This is due to the proximity of the frequencies of 1P and 3P (**Fig. 2**) loading to the natural frequency of the structure. A complete design of a wind turbine foundation, either numerically or physically, will therefore need to account for both loading conditions.

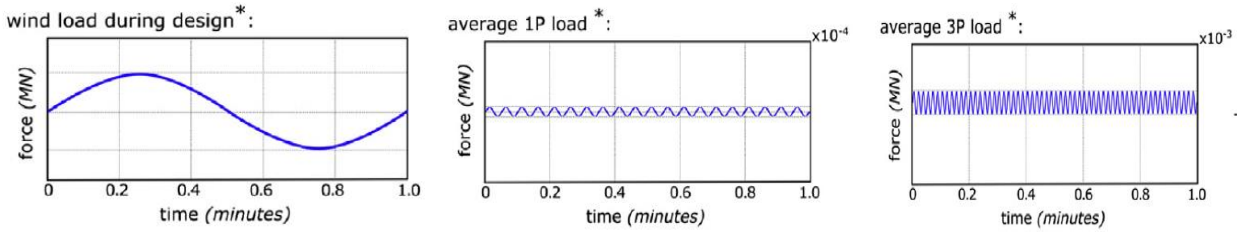

Fig. 2. Order of magnitudes of applied loads and corresponding frequency for; wind load, 1P loading and 3P loading [4].

2.2 Physical modeling

With time, the need to model larger geotechnical structures at lower costs and reduced time grew, forcing current researchers in the field of geotechnics to investigate use of scaled replicas of the original structure. It was later discovered that to replicate the failure mechanism in a real structure, the stress and stress gradients would need to be maintained between the two scales of the structure (prototype and model). To do this, the $1/\lambda$ scale model ('λ' denoting the assigned geometrical scale factor) can be tested under an acceleration λ times greater than gravity. [6] listed the various solutions devised and tested by different authors to obtain the same stress levels. Reference can be made to [7] for a detailed history of centrifuge modeling, and for a detailed history and development of physical modeling, [8] and [9] can be referred to.

In physical modeling, once the selection of a suitable similitude method has been made, similitude relationships can be formulated. The process involves the determination of scale factors to be employed on the downscaled structure. Based on previous works, there are three different 1-g model configurations; 1) 1-g model incorporating different material models than the prototype [10], 2) 1-g modeling incorporating additional loads ([11], [12], [13]) and 3) centrifuge modeling [6]. While the formulated set of similitude relationships are mainly applicable within the elastic limit, similarity relationships for strength parameters would need to be evaluated for a study at the Ultimate Limit State. But this is largely hindered by what is known as 'size effect'. Reference can be made to [14] and a more recent paper by [15] for more on the size effect.

Below is a discussion on materials used in the design of a downscaled gravity foundation overlying a soil structure as reported by previous researchers in the field of geotechnics. Due to the lack of sufficient specific studies made on physical modeling for onshore gravity wind turbines, reference is made to material models of other equivalent geotechnical structures.

2.2.1 Model reinforced concrete

In the studies by [16] and [17] on small-scale modeling of reinforced concrete, the reinforcement was reduced both geometrically and at the level of its mechanical properties. For example, [17] used lead wires of diameter 12.2 mm as a material closely matching 1/10th the tensile strength and modulus of elasticity of reinforcing steel. Direct pull-out tests were performed to test the effect of different wire configurations within the concrete. The conclusion drawn from their experiments is that achieving similitude based on yield stress by modifying the cross-sectional area is more accurate. On the other hand, [18] implemented a 1/5 scale model of a 3-story RC frame and relied upon comparing the yield forces to comply with similitude rules. [16] conducted a study on small-scale modeling of reinforced

concrete structural elements for use in a Geotechnical Centrifuge and the parameter used to match the two scales at 1:40 was the modulus of rupture of the concrete. Scaling of concrete reinforcement and aggregates were considered. The authors suggest the same modulus of rupture for the model concrete as that of the full-scale concrete to provide a good approximation. In a previous study by [17], the model building materials used had ultimate load capacities and stiffnesses of only $1/\lambda$ which resulted to stresses downscaled by $1/\lambda$ and model strains identical to those of prototype.

In full-scale reinforced structures, reinforcement bar diameters used are commonly between 16 mm and 25 mm. An equivalent structure at laboratory scale where the components are downscaled geometrically by factor $1/\lambda$ would normally require bar sizes that may not necessarily be readily available for use. Upon use of smaller bar sizes further treatment on the surface of the bar would be required to maintain similarity of the reinforcement- concrete bond as that experienced in the prototype. For example, in the study by [16], reinforcement bars were scaled down by a factor of 40 (geometrical scale factor) to stainless steel wires of diameter 0.58 and 0.26 mm. Most of these wires or mesh were roughened using Congleton HST 95 silica sand in which a fast-drying epoxy resin was used to coat the steel. However, if it is decided to use the same mechanical properties of concrete as the prototype, the same reinforcement mechanical properties should also be used.

2.2.2 Model soil

In soil mechanics, requirements to achieve similitude in physical models has been much more demanding than in other disciplines [7]. Since soils used in geotechnics are multiphasic materials consisting of the coexistence of solid grains, air and water (or moisture), complete similitude is impossible, despite the many attempts made in this direction. Reference can be made to [7] for an overview of earlier works on the subject.

Despite the challenges in attaining full similitude in soils, sandy soils are typically used to simulate the soil in a soil-structure interaction problem, as they maintain the similarity of the friction angle [19] and also because of the limited number of parameters required [7]. However, the choice of the particle size should be considered to avoid the particle size effect [6]. More details on the properties of the sand and difficulties related to material choice have been extensively discussed in [20]. However, in most cases, physical modeling should be complemented with other design methods (like numerical simulations) to achieve an acceptable level of sufficiency and reliability in the design outcomes.

2.3 Numerical modeling

In a wind turbine system, the soil undergoes alternating cycles of stresses continuously throughout its life. Under such loading conditions, the soil is known to exhibit complex nonlinear behavior [21]. Commonly used constitutive models are the Mohr-Coulomb failure criterion, the Hardening soil model, the Hardening soil-small model and the Soft soil model [22]. Amongst them, the Mohr-Coulomb model is generally considered as a first-order approximation for soil behavior due to its very limited set of parameters required. Despite its ease in use in the absence of sufficient data, Mohr-Coulomb model is not suitable for soils under loading that produces accumulated strains since it is based on one yield surface without hardening [23].

3 Calculation and experimentation

3.1 Numerical modeling

The current research study constitutes numerical simulations performed on both scales of the foundation; the full scale and 1/10 reduced scale model. The main purpose of the numerical simulation is to aid in the conceptualization of the physical model implementation. However, this section does not seek to fill the knowledge gap in the constitutive law used for wind turbines, as in this section, Linear Elastic model is used to illustrate and highlight modeling techniques. As discussed in Section 1.3, modeling of wind turbines requires more sophisticated methods to capture its true behavior depending on the type of soil and loading.

3.1.1 Description of model setup and parameters

The numerical model setup was based on the properties of an existing onshore wind turbine manufactured by one of the project partners (NORDEX) that was selected and dedicated for the purposes of the current study. The schematic in **Fig. 3** presents the general features of a wind turbine system. For numerical simplicity and due to symmetry, only half of the wind turbine was modeled. Since it would be computationally costly to model all the components of the wind turbine, in most cases, but wherever necessary, only essential features of the wind turbine meant to serve the purpose of the research shall be geometrically modelled. Other elements shall be accounted for either as external loads or simplified objects/elements. Also, to narrow down the scope of the study, only the structure's behavior in static and linear conditions are examined. However, the importance of the study of soil-structure interface under cyclic and dynamic loadings is acknowledged based on numerous reports on the importance of predicting the long-term effects of structures under repeated loading.

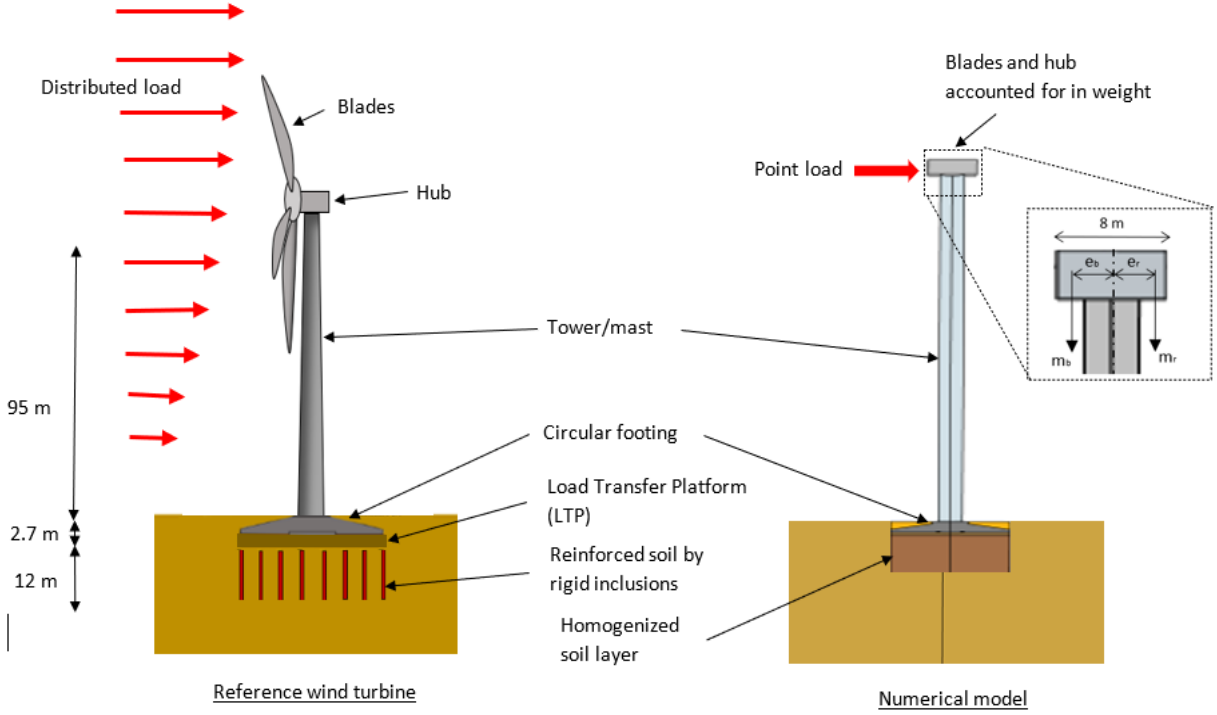

Fig. 3. Schematic of the referenced onshore wind turbine setup (real scale) versus numerical model setup.

The essential features to highlight in **Fig. 3** are the simplifications made on the loading type (distributed loading resolved and simulated as a point load), soil type (reinforced soil simulated as homogenized soil) and, blade and hub (modeled as a block of equivalent weight). It was decided to simulate the entire wind turbine for the determination of mast stresses and for comparison with the laboratory model where mast displacements are measured. The numerical model consists of a 95 m long turbine tower with a 4 m x 8 m x 2 m block of density equal to 3199 kg/m^3 attached to its top surface. The density was determined in such a way as to produce the required rotor and blades combined weight of 2,047 kN. However, the eccentricities are equal for this simulation and considering the combined weights, the moments created cancel. However, in a real wind turbine, the blade and rotor are situated at distances *eb* and er respectively from the central axis of the tower each associated with its own mass mb and *mr* as shown in **Fig. 3**.

Underlying soil

The 3D numerical model consists of two main soil layers: the Load Transfer Platform (LTP) of 0.8 m thickness overlying a 12 m reinforced soil layer (**Fig. 3**). The reinforced soil by rigid inclusions consists of multi-layered soil; however, the numerical model consists of homogenization of the reinforced system whose equivalent properties are provided by the soil experts of the project (MENARD). To limit boundary effects, the soil is modeled as a cylindrical object of 120 m diameter and 50 m depth of which 0.8 m is the LTP and 12 m is the reinforced soil. Roller supports are assigned at the bottom of the soil layer where vertical displacements are restricted and on extreme vertical

boundaries including planes of symmetry where horizontal displacements are restricted. Through numerical simulations under the load case of interest (permanent loads), the choice of the 120 m width was concluded where no boundary effects were felt.

Reinforced concrete

The numerical simulation of the reinforced concrete overlying the soil structure was modeled as a linear elastic 3D structure. In similar studies, the concrete footing is considered rigid relative to the underlying soil, therefore in essence, a failure criterion ought to be set for the soil model. The simulation consists of modeling the concrete mass using the 3D solid object similar to that used for the soil and 2D truss elements for the reinforcements. The reinforcement-concrete interaction is enabled through nodes that allow shared displacements at selected points between the contact surfaces of the concrete and reinforcement bars.

Tower, hub and rotor

The tower was numerically modelled using a shell interface available on COMSOL Multi physics© software. With this interface, the thickness of the structure is not geometrically displayed but allows it to be defined as an input parameter and only accounted for mathematically during the simulation. This makes the use of the Shell interface efficient since only boundaries are meshed and can be used to model thin structures in 3D, but only provide good results as long as the structures are thin. Also, the structural transient behavior of the shell element was set to 'quasi-static' and therefore, any inertial terms were ignored.

Soil-footing interaction

The soil-structure interaction plays a vital role in geotechnical structures, even more so under cyclic or dynamic loads. Considering failure by excessive overturning moment, the concrete structure may detach from the soil. Since the soil cannot withstand tension, and as the contact surface between the foundation and soil lessens, the superstructure would eventually succumb to failure. In the current numerical simulation, the contact surface between the foundation and the soil is modeled as a perfect contact with no possibility of separation. This is justified by the small load levels imposed on the model that would unlikely cause soil-footing detachment.

Tower-footing interaction

The simulation of the tower-footing interaction constitutes an anchor cage integrated within the reinforced concrete and attached to the tower through vertical threaded bolts. Reference can be made to **Fig. 4** below for a meshed representation of the interaction indicating the different elements forming the connection. The threaded bolts play a significant role in maintaining the interaction between the tower and the foundation. This is enabled through nuts that maintain surface contact with the flange of the tower whose contact is normally enhanced through pre-tensioning the bolts. In **Fig. 4**, the nuts are geometrically modeled whose contact surfaces with the tower flange can be modeled using a suitable constitutive model to simulate the possible loosening of the nuts during cyclic loading; however, all nut-flange contact surfaces were modeled as perfect bonds with no possibility of separation /loosening between them

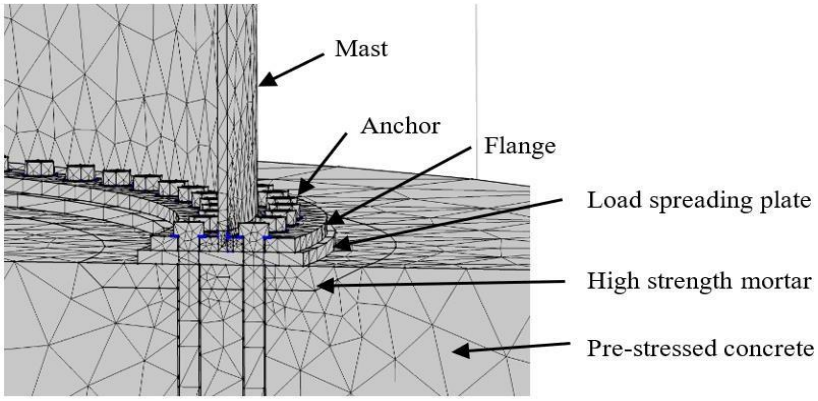

Fig. 4. Tower (mast)-footing interaction of an onshore wind turbine footing (anchored system).

The adopted configuration constitutes 80 bolts (half the total number of 160 bolts) embedded in the concrete foundation passing through the leveling layer of mortar and anchored at the top and bottom to two 6 cm-thick circular steel crowns representing the load spreading plate and the anchor plate.

Mesh configuration

The meshing is through the 'General physics-controlled mesh size' option provided by COMSOL in addition to manual refinement necessary for increased accuracy on thin elements and areas around sharp edges. For example, very thin elements on the threaded bolts and larger elements for the far field (**Fig. 5a**). The element type used is the tetrahedral element. The mesh quality was checked on the adopted mesh where a value of 1 indicates high quality mesh and 0 of low quality (a degenerated element). The histogram (**Fig. 5b**) shows the frequency of a particular mesh quality (between 0 and 1) considering all mesh elements in the model. The most frequented mesh quality is 0.65 for the simulated model as indicated on the histogram.

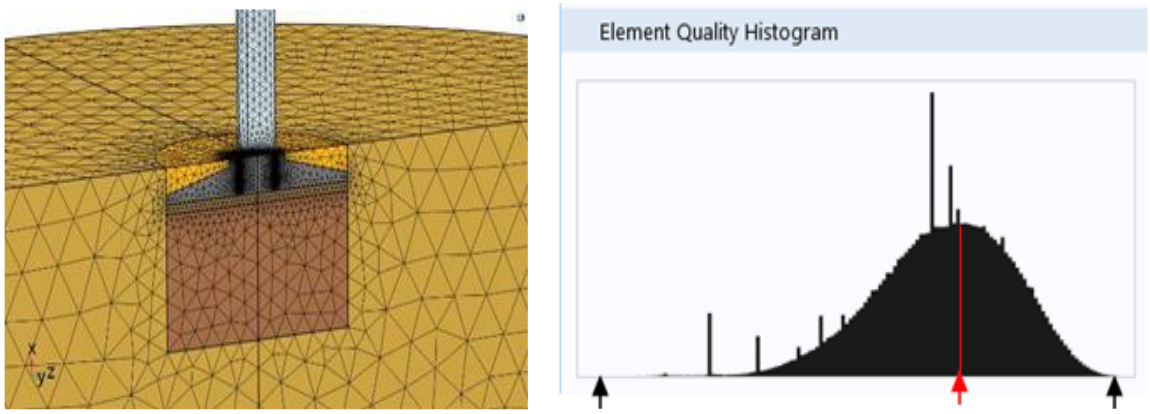

Fig. 5. a) Unstructured 3D meshing on COMSOL software and b) Element quality histogram.

3.1.2 Simulation of 1/10 small-scale model

Considering the adopted mesh and setup as described in section 2.1, the conceptualization of the small-scale model involved numerical simulations of various configurations with consideration of two main things; 1) response similar (but not necessarily the same) to those obtained in the real structure (prototype) and 2) conditions, limitations and capacity of the laboratory where the 1/10 physical model will be implemented. Initially, six simulations were performed in the process of determining the model configuration (config.) to implement:

- Prototype (tower height = 95 m)
- Fully downscaled model (tower height = 9.5 m)
- Config. a - Downscaled model (tower height=3.0 m with additional load on tower)
- Config. b - Downscaled model (tower height = 3.0 m without additional load on tower)
- Config. c - FEDRE model / implemented model (tower height = 3.0 m with additional load on tower)
- Config. d - FEDRE model / implemented model (tower height = 3.0 m without additional load on tower)

Table 1. Parameter scale factors as used in the numerical model.

Diameter (m)	Young's Modulus (GPa)	Density (kN/m^3)	Vertical load V (kN)	Moment M (kN.m)	Soil stress (MPa)	Soil settlement (m)
$1/\lambda$	1	1	$1/\lambda^3$	$1/\lambda^4$	$1/\lambda$	$1/\lambda^2$

The fully downscaled model maintains all necessary similitude laws for scale factor λ =10 using similitude relationships as reported in previous works. The downscaled models, config. a and b, are simulated since it is not physically possible to implement and test a 9.5 m tower in the laboratory. As a result, only 3 m of tower height could be implemented. However, to maintain similitude in loading, additional weight (m_{rb+t}) is added onto the 3 m high tower as a block of weight equivalent to the

remaining 6.5 m of the tower ('t') in addition to the weight of the rotor and blades ('rb'). Configurations without additional loads simply seek to quantify the effect of the additional weights. The parameter scale factors are presented in **Table 1** where λ =10.

The results of the simulation on **Fig. 6** show same levels of soil vertical displacements and stresses (negative values indicating compression) in the fully downscaled model and config. 'a' compared to those of the prototype. This further validates the similitude relationships used. However, if the 3 m tower is modeled without account for the additional loads, the level of rotation of the footing is maintained considering the applied horizontal load, however, the total vertical displacement levels are expectedly reduced by about 0.02 mm (2 mm at prototype scale). It is worth noting that the corresponding displacements for the downscaled model are 100 times less and stress values 10 times less; however, for comparisons with the prototype in **Fig. 6**, the values are multiplied by these factors respectively.

Regarding the implemented model (identified as 'FEDRE model'), the soil depth is 40 cm with Young modulus of 60 MPa obtained through a dynamic plate load test performed on the model soil. The rotation of the implemented footing is significantly less relative to those of a fully downscaled soil depth. This is due to the influence of the relatively rigid floor compared to the reinforced soil in real conditions.

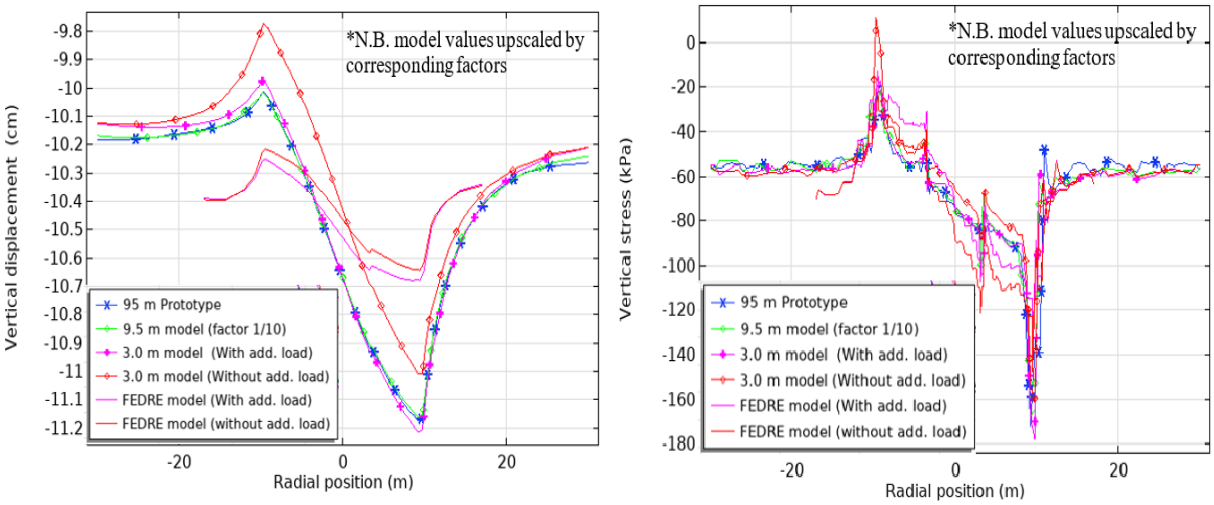

Fig. 6. Simulation of 1/10 scale physical model of varying configurations, a) Vertical displacements and b) Vertical stress.

3.1.3 Model configuration based on additional loads on soil and footing (σsoil_model ~ σsoil_real)

Based on reports of previous research works, same soil stress levels as those of the prototype can be reached by incorporating additional masses into the physical model. The additional mass is essentially the difference in mass of a model whose density (or gravitational force) is λ times more than that of its prototype to that whose density is maintained as that of the prototype. In this section, the compensation of mass of the footing shall be referred to as *M*f, of the backfill soil, *M*s and that of the mast, *M*m.

Considering the model soil of 40 cm depth and stiffness of 60 MPa, two main model configurations are simulated. The simulation of the first configuration is after [24] and involves no additional loads resulting to λ times less resulting stress than the full-scale structure. The second configuration is after [10] to [13] that incorporates additional loads in an attempt to obtain soil stresses in the same order of magnitude as the full-scale structure. In this study, the first and second configurations shall be referred to as configurations 1 and 2 respectively. While configuration 1 maintains the general geometry of the real structure and can be considered as a complete similitude, it is limited to comparisons with the real structure within regions where linear elasticity can be safely assumed. This is due to relatively low loads that can be applied (as a result of the same material strength as prototype but λ times less weight than required for the model), and therefore, behavior at Ultimate Limit State cannot be studied. The configuration is mainly dedicated to the study of the distribution of loads from point of load application

to the soil under the chosen test setup. In the case of similitude configuration 2, the behavior of the soil under failure loads can be studied.

Scale factors description

The scale factors used in the implementation of the two similitude configurations are those presented in **Table 2**. It can be seen that incorporating additional loads allows for the larger applied moment. While the factors presented are based on theoretical formulations, testing their applicability under numerical and physical conditions forms one of the objectives of this study.

Table 2. Theoretical parameter scale factor for two model configurations.

Parameter	Model configuration 1	Model configuration 2
Diameter (m)	$1/\lambda$	$1/\lambda$
Stiffness (GPa)	1	1
Density (kN/m^3)	1	1
Vertical Load (kN)	$1/\lambda^3$	$1/\lambda^2$ (incorporates additional load of factor $= 1/\lambda^2 - 1/\lambda^3 = 1/\lambda$)
Moment (kN.m)	$1/\lambda^4$	$1/\lambda^3$
Soil stress (MPa)	$1/\lambda$	1

Additional load for concrete foundation, backfill and mast

The theoretical additional load required is based on Equation 1 below where $M_{f,s}$ is the compensation mass (required additional mass) for both the concrete footing and backfill, M_{total} is the theoretical total mass required corresponding to mass factored by λ_2 and m is the mass of footing and backfill. In this study, the compensation of mass is intended for both the concrete foundation and the backfill (in addition to that of the mast). This is due to the significant contribution of the backfill on the mass of the footing.

$$M_{f,s} = M_{total} - m \tag{1}$$

Considering the volume and density of the downscaled concrete footing and backfill, the total weight 'm' is of 2 tons and M_{total} of 20 tons, Equation 1 therefore proposes an additional 18 tons of mass evenly distributed on the foundation at ground level to prevent any overturning under the applied load corresponding to factor of λ_2. Practically, a total additional load of 13.8 tons was possible and was therefore implemented in the laboratory. The mass was limited by an attempt to maintain symmetry in loading as much as possible at the closest mass possible to the theoretical mass of 18 tons.

The implemented additional load constituted a total of 6 concrete blocks each of dimensions 0.8 m x 0.8 m x 1.6 m weighing 2.3 tons. An image of the numerical setup is shown on Figure 7. In addition to maintaining symmetry, the placement of the additional load was in such a way to prioritize the surface directly above the concrete foundation. This therefore necessitated placement of a circular steel ring of 1.5 cm thickness below the additional masses. The steel ring is considered rigid in relation to the applied load and therefore allows for a more evenly distributed loading onto the foundation. The circular shape is intended to maintain the circular nature of the load distribution under the concrete foundation. Due to the presence of LVDT in the physical model, the setup of the concrete blocks is limited to the configuration as shown in **Fig. 7**. Similarly, the weight of the superstructure required mass compensation for similarity requirements.

Following the determination of required additional ('add.') loads, numerical simulations were performed to test their effectiveness on achieving similar soil stress levels as in the prototype. Four model setups were simulated and compared with the reference and FEDRE model:

- Reference model
- Setup 1 – Add. weight for footing, backfill, surrounding soil and mast
- Setup 2 – Add. weight for footing, backfill and surrounding soil
- Setup 3 – Add. weight for footing and backfill
- Setup 4 – No additional load
- FEDRE model / Implemented model

Setups 1 to 4 are considered geometrically fully downscaled with a violation only on the similitude in mass where additional masses are incorporated to counter this violation.

Due to non-symmetry in the placement of the additional load on the implemented model, modeling half the structure was no longer feasible and a full 360° 3D model had to be simulated. Since the mast height is less, a horizontal load of 15 kN was applied to produce a moment at the foot of the mast (=4.5 kN.m) close enough to that of the reference model (=4.6 kN.m).

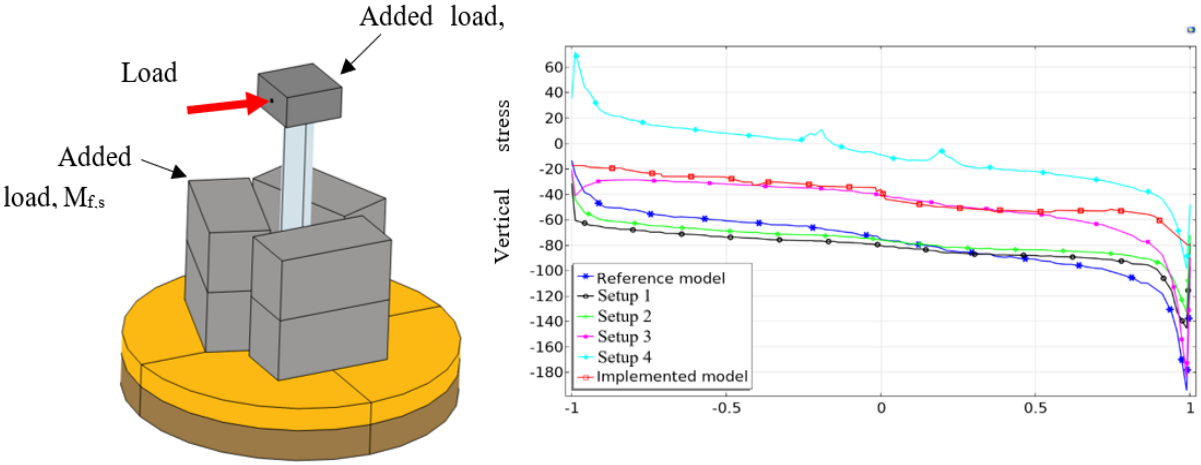

Fig. 7. a) Implemented model configuration, b) vertical stress on underlying soil at depth d=- 0.4 m below the bottom of footing due to eccentric loading.

A general interpretation of the results concludes on the usefulness of the additional load in achieving the same levels of soil stress similar to in-situ stresses. This is shown through similar stress levels in setups 1 and 2 compared to those of the reference model; while in the absence of the additional load, tensile forces are developed in the soil indicating detachment of the footing from the soil if a failure criterion had been set at the contact surface (possibility of debonding). Furthermore, the model implemented in the laboratory is also shown to achieve the same levels of stress as the reference model.

A more thorough interpretation identifies a better approximation to the reference model if all components are accounted for in weight; footing, backfill, mast and surrounding soil. This is shown by the noticeably closer stress levels of setups 1 and 2 to the reference model. It is worth restating that the stresses of the reference model are the same as those of the real structure, and therefore, setups 1 and 2 achieve soil stresses as in real scale conditions.

3.2 Physical modeling

This section presents the results of an experimental program with two main objectives; 1) to test two configurations of similitude relationships as described in the numerical modeling section and 2) to determine potential critical points in the footing and soil through sensor measurements due to application of eccentric loading as experienced in real onshore wind turbine foundations.

3.2.1 Adopted loading sequence

The choice on the loading scheme was based on initially subjecting the model to an overturning moment at the top of the footing (bottom of mast) equivalent to the quasi-static design moment of the real structure. The wind load is simulated as a one-way, force-controlled lateral load applied with a sinusoidal character of 0.1 *Hz* (T=10 s). Firstly, few cycles of quasi-static loading were applied on the configuration with no additional loads with application of very small loads to not cause overturning and to maintain elastic conditions. This was mainly to determine critical points in the system (mast, footing and soil). Upon incorporating additional loads, monotonic loading was applied up to occurrence of failure.

For configuration 1 (without additional loads), the 3 m tall model should be subjected to a 1.5 kN of horizontal load to obtain the downscaled moment of 4.5 kN.m at the level of the concrete foundation

as described in the section 2.3.2. However, 2 kN load was applied on the physical model for practical purposes. This theoretically produces a 6 kN.m moment at the top of the footing.

3.2.2 Implementation process of small-scale laboratory model

Reinforcement and anchor cage

Considering reinforcement bars of averagely 20 mm diameter in the real footing, theoretically downscaled bars should be 2 mm (λ=10). Practically, a 2 mm bar commonly referred to as a welded wire fabric or a wire mesh, would lack surface properties that are essential for the steel-concrete bond and therefore, for the current physical model, the minimum readily available threaded reinforcement bar was used; in this case, a 6 mm bar. The reinforcement design using 6 mm bars was based on maintaining the total cross-sectional area as that if 2 mm diameter bars were used. This may be acceptable for a study within the serviceability limit state where crack patterns do not form part of the research objective.

Fig. 8 presents the reinforcement ratios in cm^2/m along the foundations' radius. Reinforcement ratios of the bottom radial bars and the shear (vertical) bars are shown for both the real scale and the laboratory scale. It is worth noting that since the factor of the ratio 'area/length' is λ, the laboratory model values are multiplied by λ for comparison purposes. An over-estimate of the volume of reinforcement in the laboratory model can be observed; however, the general shape of the reinforcement requirement across the radius is maintained.

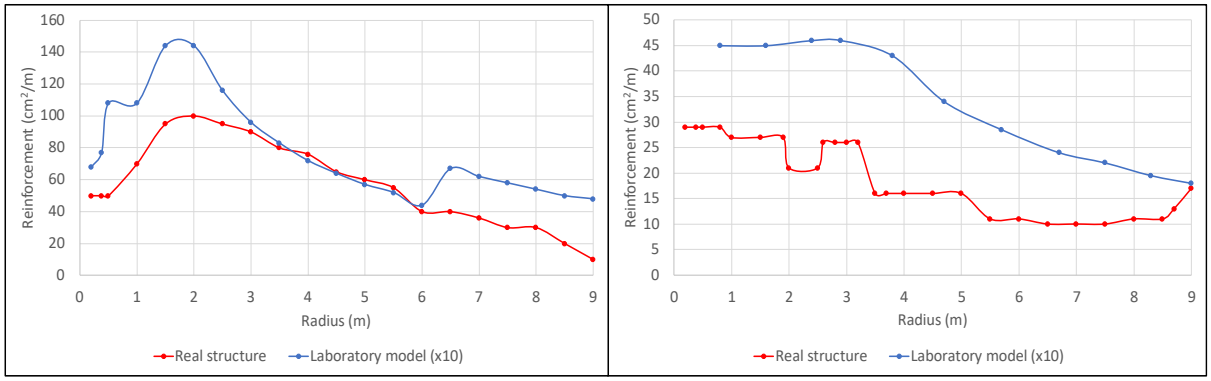

Fig. 8. Reinforcement ratios of laboratory model versus real structure; a) Lower radial bars and b) shear (vertical) bars.

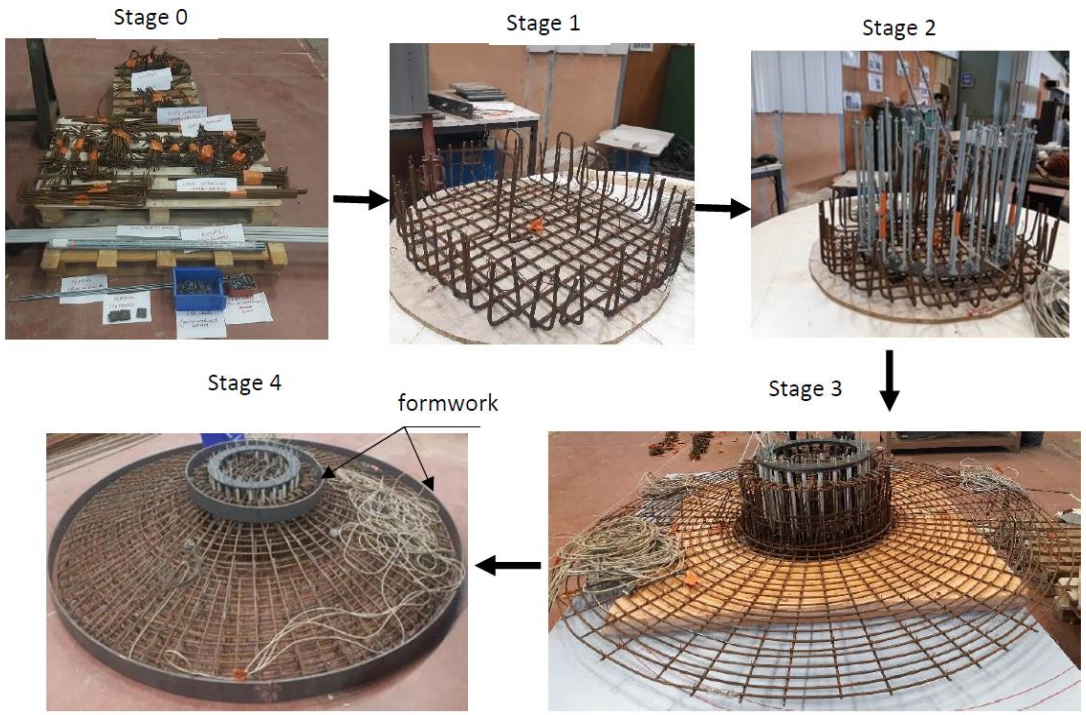

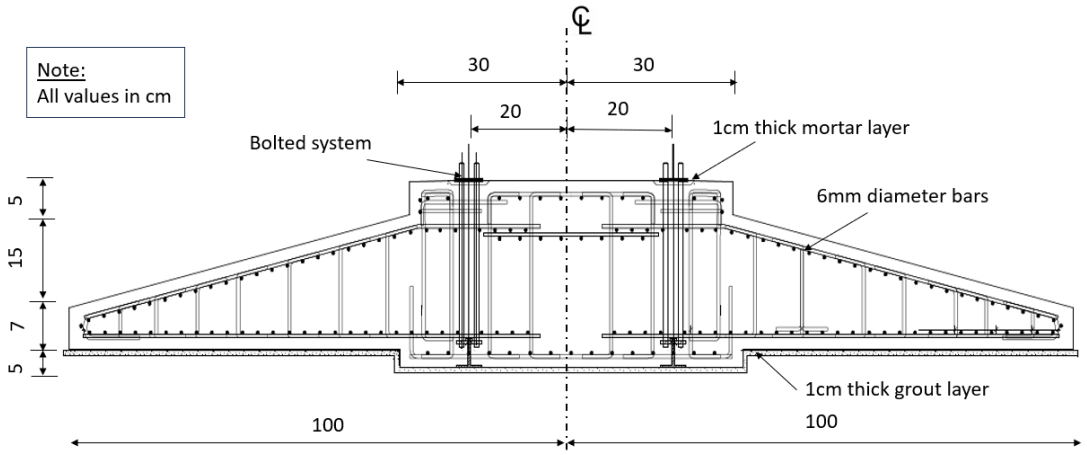

Fig. 9. Reinforcement and anchor cage layout and implementation process (stages 0 to 4).

The anchor cage of the physical model constitutes a total of 48 anchor bolts of 8 mm diameter (M8 threaded bars) protruding from the foundation and connecting it with the S355 steel tower mast. The total number was initially chosen based on the equivalent stress felt underneath the load spreading plate. Real images of the implemented reinforcement and anchor cage is as shown in **Fig. 9**.

Underlying soil

The underlying soil is 0-4 mm sand compacted at a moisture content of 5% to a total thickness of 40 cm. The soil was compacted once at the final layer using a mechanical compactor to prevent over compaction of lower layers of the soil structure; a common occurrence if compacted at several layers. **Fig. 10** presents real photos of the soil setup.

Normal concrete, lean concrete and high strength mortar

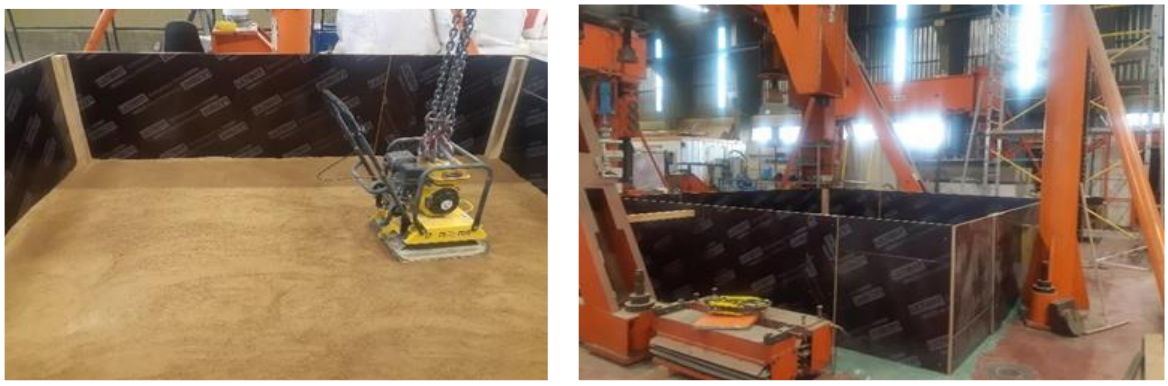

Fig. 10. Real images of; a) the soil wooden casing and b) compacted soil.

Fig. 11. Implementation of 1/10 scale reinforced concrete footing; a) 20 days after casting and b) mortar casting under load spreading plate

Before concreting of the reinforced footing, 10 MPa lean concrete of 1 cm thickness was laid. This formed a horizontal surface onto which the reinforcement cage could be placed and subsequently the

concrete footing. Therefore, it is through the bottom surface of the lean concrete that the soil-structure interaction is enabled. During pouring, a reservation was made for a 1 cm thick mortar layer below the load spreading plate as shown in **Fig. 11**. The reservation constituted placing a 1 cm thick wooden concentric plate of dimensions equal to the hardened mortar.

The high strength non-shrinking mortar was produced and managed by one of the project partners, PAREX. Similar to the procedure followed for the real foundation, the load spreading plate was fixed in place allowing maximum possible contact with the mortar as it flows beneath it and cures. Following the curing of the high strength mortar, the threaded bars were post tensioned along their whole length through a mechanical torque wrench. The mortar and threaded bars formed essential parts of the tower-footing interaction.

Backfill and placement of the mast

The backfill constituted the same soil properties as the underlying soil and a cylindrical tube of 5 mm thickness and 3 m height was connected to the concrete footing through the bolted system ('the anchor cage') (**Fig. 12**). This constituted the superstructure through which a horizontal load simulating the wind load was applied.

Fig. 12. Superstructure of the 1/10 scale model; a) Before placement and b) after connection to the footing through a bolted system.

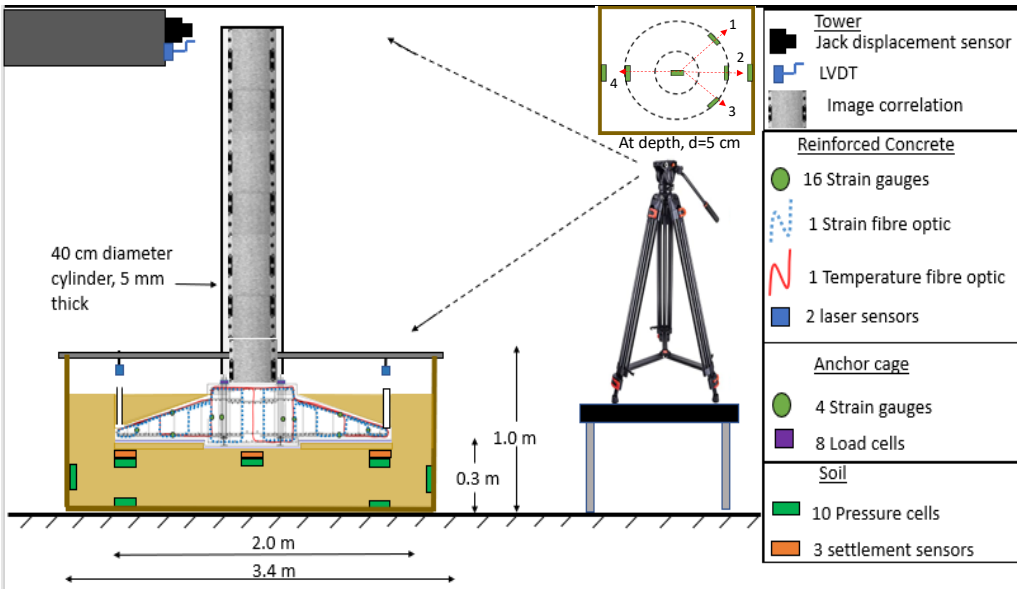

Fig. 13. Instrumentation setup of 1/10 physical model.

3.2.3 Instrumentation

Data capturing was done during the different stages of construction; from pouring of concrete to application of the quasi-static loading. The schematic in **Fig. 13** presents the positioning of all the sensors incorporated in the physical model. Sensors were placed in four principal directions suggested by the pressure distribution underneath an eccentrically loaded circular footing.

3.2.4 Characterization of model soil and concrete

The dynamic plate load test was conducted at three measuring locations. An average EV2 value (deformation modulus) of 60 MPa was determined and an average Sm value (settlement value) of 0.68 mm constituting standard deviations (SD) equal to 1.3 MPa and 0.02 mm respectively. For the purpose of numerical modeling in the current study, an EV2 value is considered as the Elastic Young's modulus and is therefore inputted on COMSOL Multiphysics for simulations within the elastic limit. However, due to the stress dependency of soil, the EV2 value may not in all cases equate to the Elastic Young's modulus. Other tests such as penetrometer soil tests and concrete compressive strength tests were conducted but it is only the elastic properties that were directly applicable to the results presented in this paper. Mohr Coulomb model for the soil and damage model for concrete shall be incorporated and presented in a subsequent document where strength parameters determined from laboratory and in-situ tests shall prove useful.

4 Results

4.1 Model configuration without additional loads (configuration 1)

The set of similitude law that results in stress and strain values of magnitudes λ times less than their prototypes is tested and results are discussed. This includes response at each loading stage; from static loads of the concrete foundation and backfill to quasi-static loading.

4.1.1 Self-weight (Concrete foundation, backfill and tower)

Fig. 14 presents pressure cell measurements due to the overlying weights of the footing, backfill and superstructure in comparison to numerical simulations. Results of vertical stress due to footing weight only show an increase of 3.2 kPa of stress exerted on the pressure cell located near the center of the foundation (PCcentre) while minimal stresses of averagely 1 kPa are experienced in the peripheries of the foundation (PC2 and PC4). Comparisons with numerical simulations show a fairly good pressure level prediction of about 4 kPa compared to 3.2 kPa by the pressure cell sensor. However, a rather significant difference can be observed at the peripheries where higher-pressure values of about 2.5 kPa is numerically predicted at exactly the footing's perimeter compared to 1.2 kPa obtained from the pressure sensors near the perimeter. The difference may be due to the positioning of the sensor based on that determined numerically where stress values quite abruptly change at the edges of the footing making it difficult to compare. The effect of the weights of the backfill and superstructure is also well simulated where a 6.5 kPa pressure is recorded by the pressure cell PCcentre compared to a 7.7 kPa vertical stress obtained through numerical simulations.

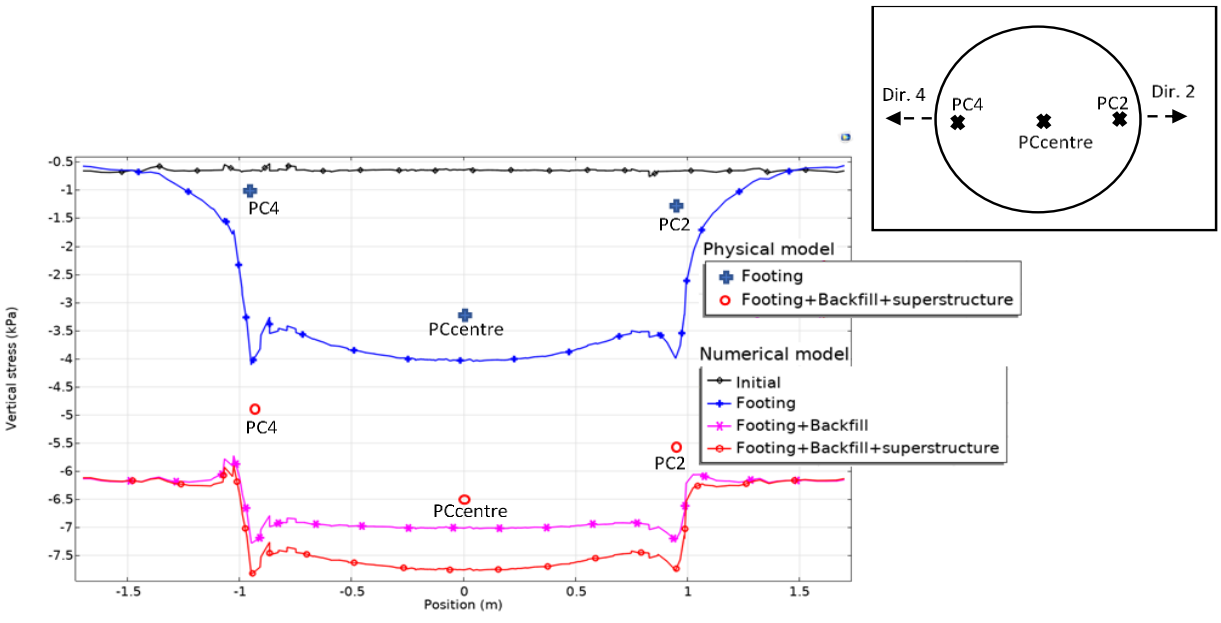

Fig. 14. Vertical stress at each construction phase of the physical model.

4.1.2 Pre-loading

Fig. 15 shows measurements of 8 load cells during the pre-loading phase. Considering the required load of 3.5 kN on each bolt based on the pre-load formula provided by the project's structural engineers, the actual load applied on the bolts varies between 1.7 kN and 5 kN. This discrepancy may be due to the influence of the preload on a bolt on neighboring bolts, which poses difficulties in maintaining the required preload. In addition, access to the inner bolts was limited due to the presence of the lower part of the cylindrical tube. Therefore, it was necessary to use a 15 cm long torque wrench extension to apply the preload to the inner bolts. This may have resulted in the lower values of 1.7 kN and 2.1 kN produced by the inner load cells.

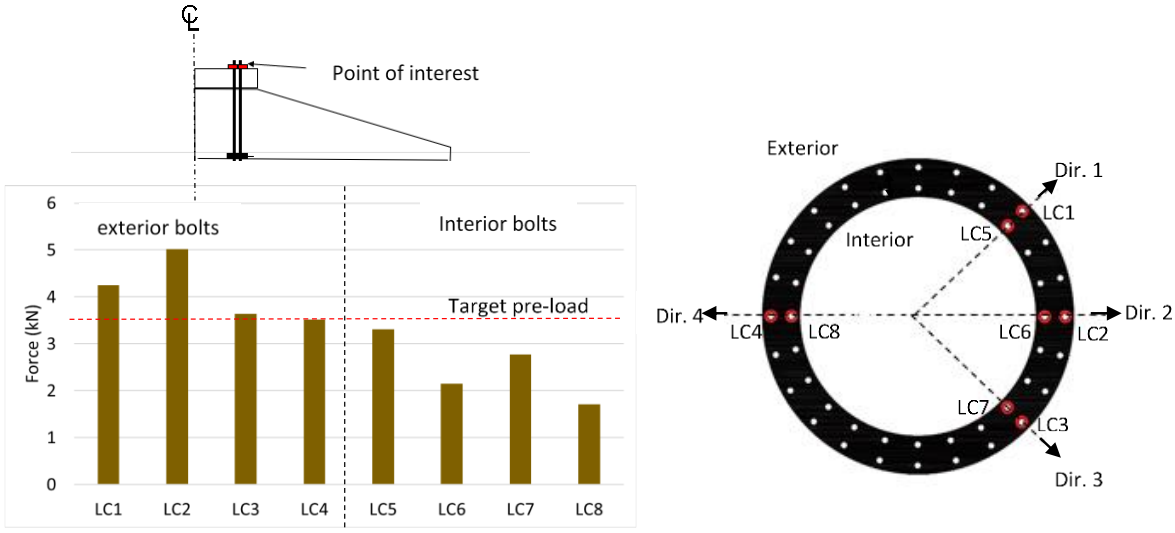

Fig. 15. a) Load captured by load cells during pre-load phase and b) plan view of load cell positions on flange of tower (mast).

During the preload phase, strain measurements in the reinforced concrete were also captured through a 12 m long fiber optic interrogated by the ODiSI 6100 which uses the OFDR (Optical Frequency Domain Reflectometry) technique based on Rayleigh scattering. Before a discussion on the recorded results, an interpretation of the targeted/intended measurements of the fiber optic is deemed necessary. This involves identifying interaction surfaces between the measuring device and its host material and assumptions on the transfer of load across this surface and highlight assumptions made for comparison with numerical simulations.

The fiber optic is attached to the bars but assumed to follow the displacements of the concrete. This is solely a result of the placement method adopted where in the case of the fiber optic, the movements of the fiber optic are considered free from the movements of the steel bars ($\Delta\varepsilon_s$) but strained from those of the concrete (**Fig. 16 b**). Therefore, the fiber optic strain ($\Delta\varepsilon_{f.o}$) are considered approximate to those of the concrete ($\Delta\varepsilon_c$). Points of interest for analysis and comparisons are as shown in **Fig. 16 a**.

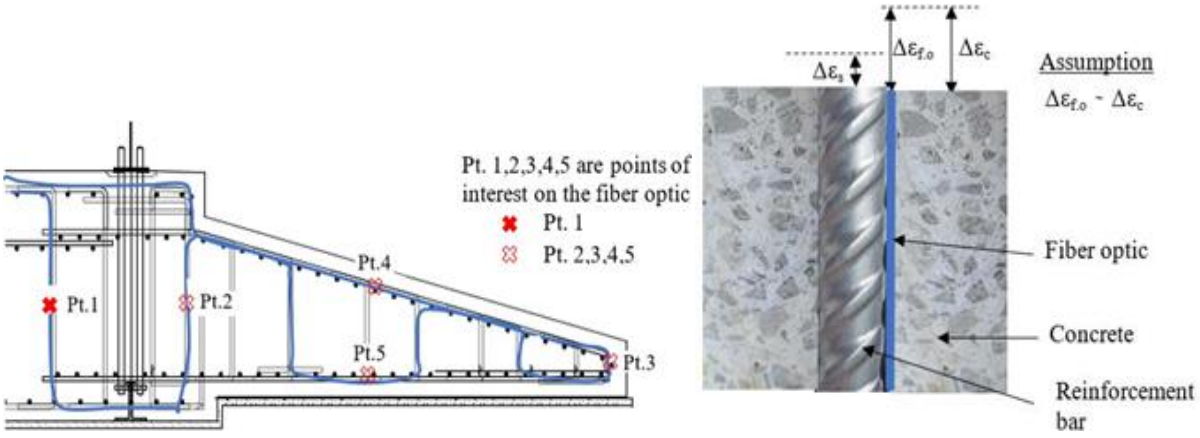

Fig. 16. a) Positioning of the fiber optic and b) contact surfaces between fiber optic and host material.

When the preload on all bolts was fully applied, the value of the strain at all points within the concrete measured along the optical fiber is presented in **Fig. 17 a**. It was noted that all peaks along the fiber optic correspond to points located within the vicinity of the anchor cage at Pt. 1 as presented on **Fig. 16**. Furthermore, the peaks correspond to positions in all the four principal directions presenting the highest response to the preload producing maximum strains of about -4 με (contraction), while points located further away from the anchors, intuitively show no response to the applied load. This is in correspondence with strains obtained numerically whose strain distribution at the central part of the anchor cage show the highest response to the preload (**Fig. 17 b**).

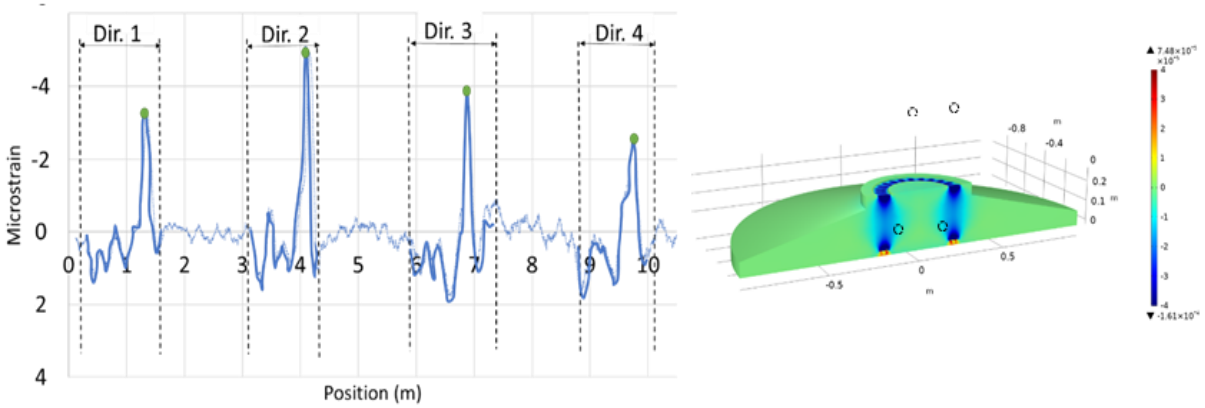

Fig. 17. Strain measurements due to preload; a) along the length of the fiber optic at time when the preload is fully applied and b) numerical simulations.

4.1.3 Quasi-static loading

Mast displacements

The application of 2 kN loading amplitude solicited at a loading frequency f=0.1 Hz resulted to a maximum mast displacement of 2 mm. The level of reliance on the displacement measurements provided by the jack's built-in displacement sensor was enhanced by an LVDT sensor positioned at the same point. The behavior of the mast under the applied horizontal load is completed by the Digital Image Correlation (DIC) technique.

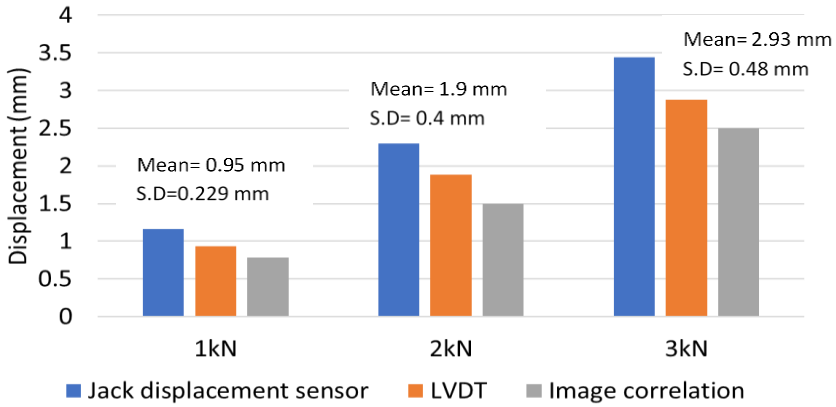

Fig. 18. Comparison of maximum mast displacement captured by three measuring devices; jack displacement sensor, LVDT and image correlation.

The results of the image correlation are presented on **Fig. 19** where a maximum mast displacement ('dm') of 1.4 mm and a minimum displacement of 0.2 mm is observed at the top and bottom of the mast respectively. A comparison is made with numerically obtained contours of mast horizontal displacements where, at maximum displacement, the numerical simulation deviates from the sensor measurement by 14 %. Furthermore, a comparison of the results of the three displacement measuring devices are presented on **Fig. 18**. Considering the LVDT as the most accurate of the three, an error of 1% and 0.7% exists upon comparing the LVDT measurements to the image correlation and the jack

displacement measurements respectively. The mean values and standard deviations (S.D) are provided for 1 kN, 2 kN and 3 kN of applied horizontal load.

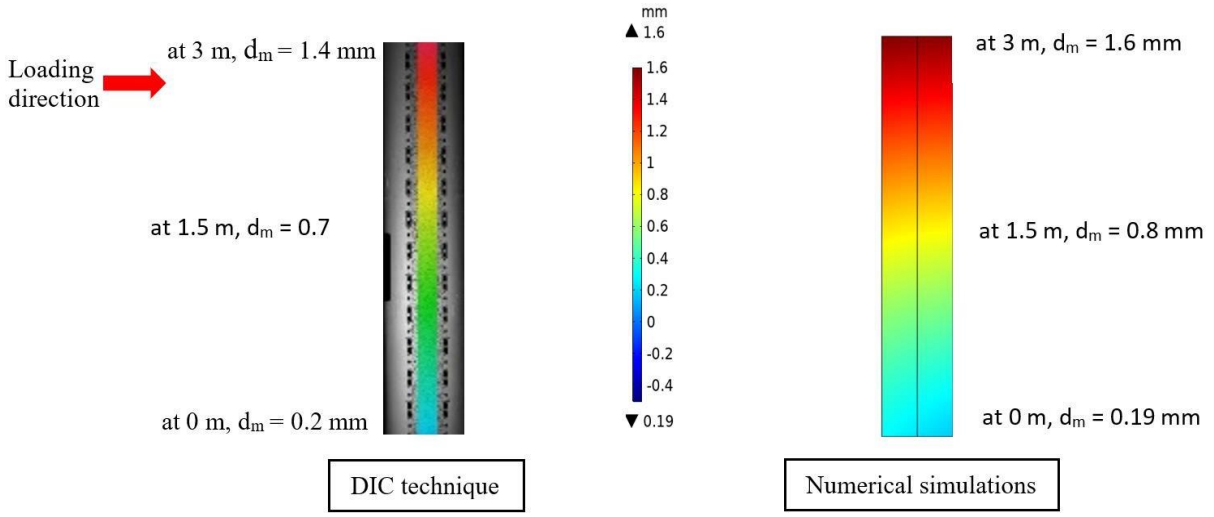

Fig. 19. Mast displacement 'dm' for 2 kN loading; measurements by DIC technique versus numerical simulations.

Strains in footing by fiber optic technology

In addition to the mast displacements, strain measurements in the reinforced concrete were captured through the fiber optic during quasi-static loading. Following the assumption of a perfect bond between the fibre optic and its host material, the interpretation is made by considering the measured strains at the load amplitude of 2 kN and comparisons with numerically obtained principal strains at this loading. For a clearer perception of the response, the Young modulus of concrete Ec of the physical model is assumed using a typical value of 30 GPa. However, it is worth noting that the Young modulus remains unknown and assumptions using typical concrete Young's modulus may lead to misleading stress results in design, and therefore an appropriate comparison would be at strain level. But to provide a sense of the order of magnitude concerning the concrete strength, stress values are presented.

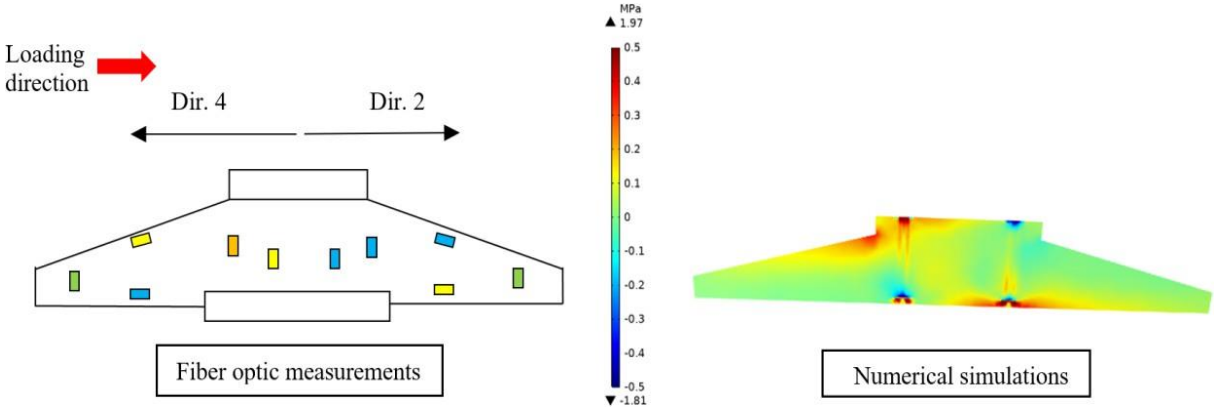

Fig. 20. Stress in concrete footing for 2 kN loading; fiber optic measurements versus numerical simulations.

Fig. 20 presents the principal stress levels in the physical model and numerical simulations at the axis of symmetry through directions 2 and 4. Since the results present the effect of the 2 kN load only; strictly in this discussion, compression shall denote negative change and tension denote positive change. A qualitative comparison of the two prediction methods (through sensors and numerical simulations), shows similar behavior in the distribution of stresses within the concrete. Generally, the two methods capture compression and tension at Pt.4 and Pt.5 in opposing directions 2 and 4 respectively (Refer to **Fig. 16** for positioning). At both Pt.1 and Pt.2 in direction 2, compression can be observed while in direction 4 at the same locations, the concrete undergoes tension. Quantitatively, slightly higher

compressive values are captured by the fiber optic compared to numerical simulations. However, considering both prediction methods, stress values less than 2 MPa both in compression and in tension are captured. This may not pose a problem for the concrete's safety in compression considering its strength of averagely 40 MPa but may pose a problem in tension considering its weakness in tension.

Soil stress by earth pressure cells.

Despite the differences in magnitude in the fiber optic and numerical simulations, the values obtained by the two methods still fall within the same order of magnitude. The reliability of the fibre optic is therefore witnessed in this aspect. However, a second model of the same structure, implementation process and loading should be tested to offer further validation to the current results.

Footing differential displacements

The footing's differential displacements were captured by LVDTs placed on extreme ends in the direction of loading. Comparisons with numerical simulations show similar displacements at positions LVDT2 and LVDT4 in directions 2 and 4 respectively (**Fig. 21**). While the LVDTs produce maximum displacements of 0.04 mm, the numerical simulation produces 0.035 mm; a good correspondence is observed. Since the LVDTs were placed only on extreme ends of the footing, comparisons with the numerical simulation are made on these points despite the numerical simulation offering full surface displacement contours.

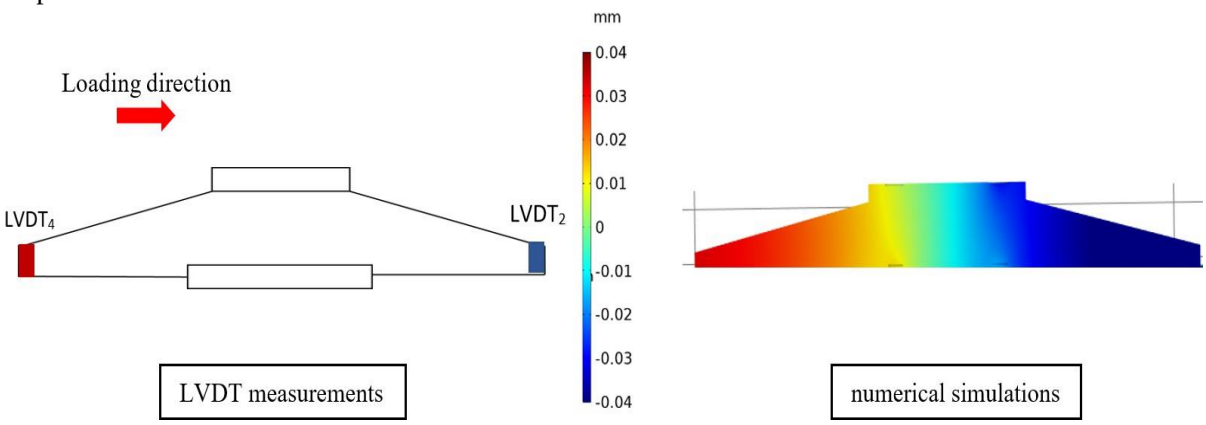

Fig. 21. Footing vertical displacements for 2 kN loading; LVDT measurements versus numerical simulations

The response captured by the pressure cells due to the 2 kN eccentric load shows pressure changes of about 6 kPa in directions 2 and 4 produced in alternating directions (**Fig. 22**). However, the pressure cells intended to capture change in pressure at the central axis show relatively non-negligible change in pressure (ΔP=2 kPa). In addition to the magnitudes, the direction of pressure change is in the opposite direction to the applied loading, similar to PC4 in direction 4.

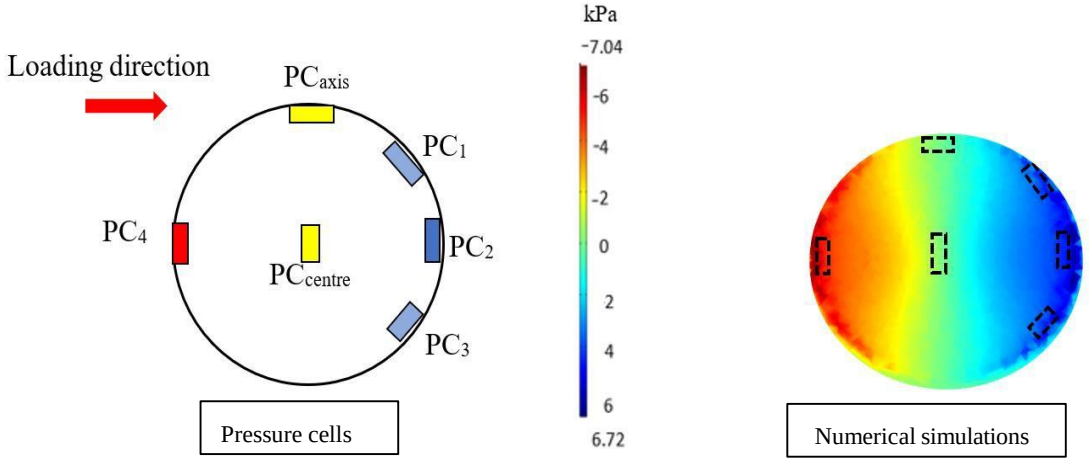

Fig. 22. Pressure measurements at d=5 cm below the bottom of footing (Plan view); Pressure cell measurements versus numerical simulation.

Upon comparisons of the pressures obtained from pressure cell measurements against those obtained through numerical simulations, there exists quite a good agreement in the results of the two prediction methods. A maximum compression increases of about 6 kPa is observed in direction 2 and a 5 kPa decrease in direction 4 in both methods. Directions 1 and 3 constitute a symmetrical increase of 4 kPa. While the maximum and minimum change in pressures in directions 2 and 4 match across the two prediction methods, the pressure experienced near the central axis measured by PCcenter and PCaxis slightly differ. This may be due to their positioning concerning the true central axis of the footing or difference in the Young modulus of soil.

Fig. 23 presents the pressure values across the depth of the soil. A comparison with numerical simulations shows a similar range of values under the load considered. Some boundary effects are felt at the extreme vertical ends of the setup but as low as 1 kPa measured by pressure cells but slightly higher in the numerical model. A second model may need to consider a wider casing.

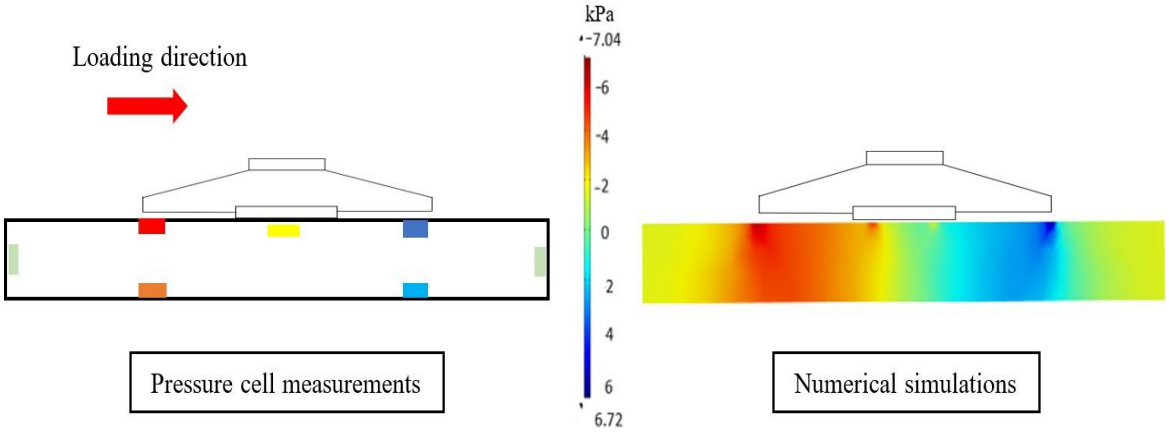

Fig. 23. Change in pressure measurements across soil depth; Pressure cell measurements versus numerical simulation.

A summary of the sensor measurements against those obtained through numerical simulations is presented in **Fig. 24**. While this offers knowledge on the load distribution in terms of tower and footing displacements, and soil pressure, a more specific study of the footing and its interaction with the mast is made possible through the strain distribution offered by the fiber optic and load by the load cells as presented previously but not presented here for clarity.

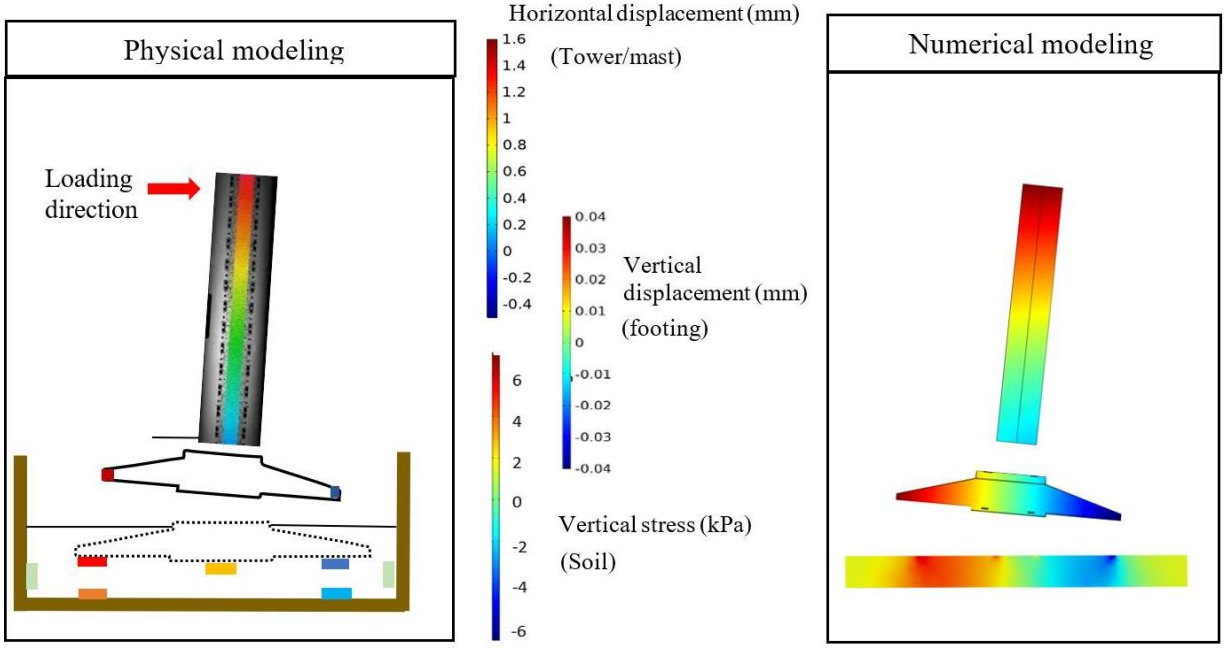

Fig. 24. Load distribution from mast to underlying soil; Sensor measurements versus numerical simulation

4.2 Model configuration based on additional loads (σsoil_model ~ σsoil_real)

A total additional mass (termed as $M_{f,s}$) of 13.8 tons was introduced into the laboratory model to compensate the reduced masses of the footing and the backfill required for similitude (**Fig. 25**). Since the additional weight is about 75 % of that required for similitude of scale factor λ=10, results of the test are used as a form of gauging the extent to which in-situ stresses are reached based on sensor measurements in the soil. The additional mass of the mast (Mm) constituted 5 rectangular plates each weighing 200 kg. In addition to the mass of the mast of 200 kg, total vertical load V on the foundation was equal to 1.2 tons. The loads were securely placed on the mast and held by a chain attached to a rigid beam. The chain is only for security purposes and hence does not contribute to any forces under the loading conditions of the test.

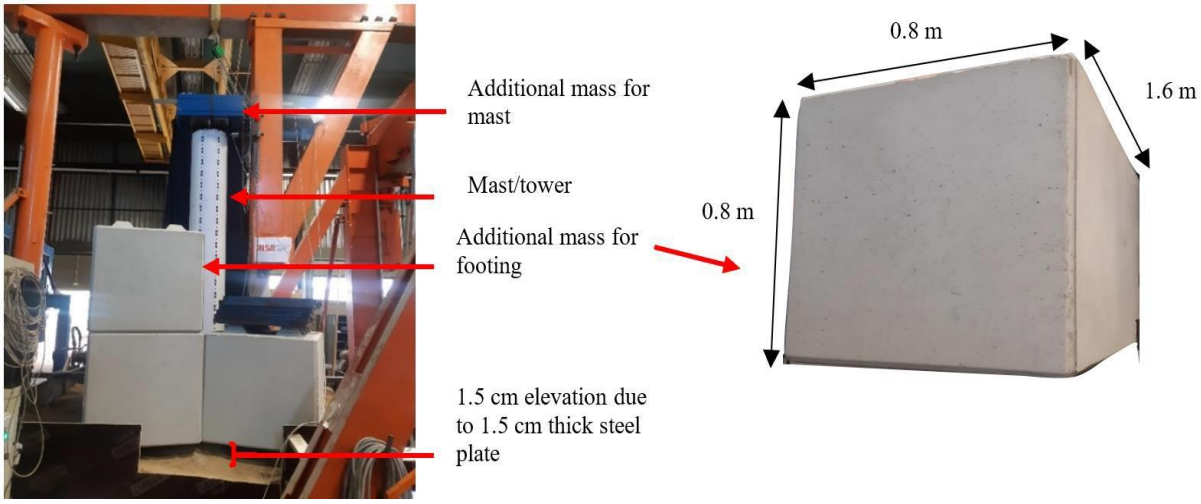

Fig. 25. Real photos of the final set-up of the physical model with additional loads for the mast and the concrete footing.

Considering the pressure cell sensors at depth d = 5 cm, the increase in pressure due to the 13.8 tons of concrete weight is as shown on **Fig. 26**. Symmetry is expected, however, the slightly lower increase of pressure in cells PC2 and PC4 reflects the lower load directly on top of the two pressure cells in directions 2 and 4 as a result of the configuration. However, an even distribution is observed through the remaining four pressure cells at this depth producing an average increase of 25 kPa. Essentially, the stress increase due to the 13.8 tons load should be nearly λ-1 times more than that caused by the weight of the reinforced concrete foundation. This is the key feature of the transition from the configuration without additional loads (configuration 1) to that constituting additional loads (configuration 2).

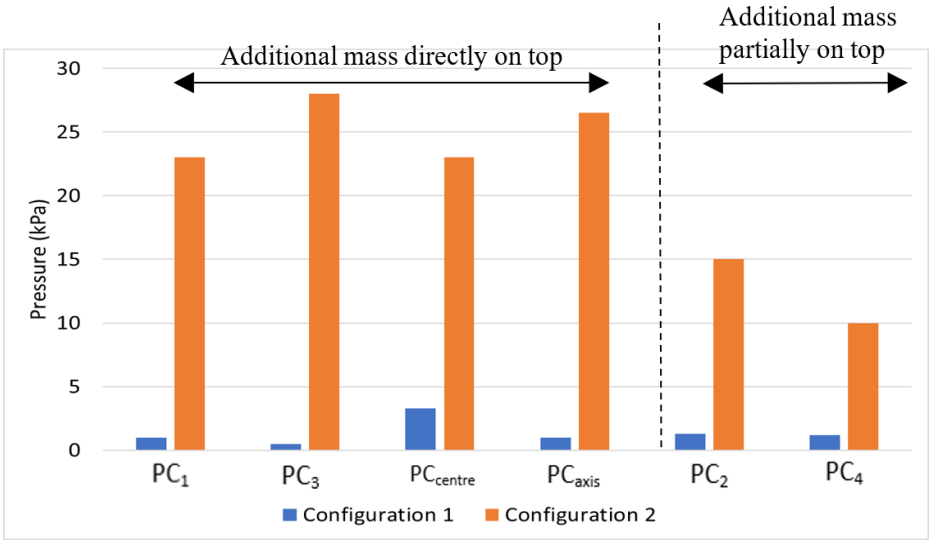

Fig. 26. Pressure increase resulting from the additional load.

Considering the pressure cell reading at the central axis of the foundation due to the placement of the concrete blocks only (producing 23 kPa of pressure) and that due to the self-weight of the concrete foundation (producing 3.2 kPa of pressure), λ-1 times the 3.2 kPa of pressure results to a theoretical 28.8 kPa of additional pressure due to the additional mass. The 20 % difference in the pressure measured by the pressure cells to that theoretically obtained is probably due to the 25 % less mass applied than that required for similitude. Upon comparing the model's pressure increase to about 28 kPa due to the weights of the concrete blocks and the footing itself, to that due to the footing weight of a real wind turbine obtained numerically as equal to averagely 25 kPa, in-situ stress values are reached by the additional loads.

4.3 Cyclic and quasi-static loading

Configuration 2 is determined assuming similarity relationships hold as presented in Table 2. However, since the relationships are derived assuming elasticity, results may be misleading/unrepresentative for values near the failure load. However, upon use of the similitude relationships for force F in configuration 1, an equivalent force in configuration 2 would require λ times the force F (hence 10F in this study). In other words, for F_1=2 kN in configuration 1, configuration 2 would therefore constitute force F_2=20 kN. For cyclic loading in this section, 50% of this load is considered, thereafter, from a monotonic loading up to failure, the true failure load will be determined.

Only results of the LVDT and pressure cell measurements are analyzed and discussed as similarity in stress in this configuration is limited to soil-structure interaction only and not the internal behavior of the footing. Furthermore, due to the well-known non-linearity of soil, the linear elastic model used in the numerical simulation shall not be compared to the sensor results due to expected higher levels of stress in the soil and a possible significant change in deformation modulus. Comparisons of results shall therefore only be made with the sensor results obtained in configuration 1.

4.3.1 Pressure cells

Changes in pressure measurements due to seven load cycles of amplitude 10 kN are plotted in **Fig. 27** corresponding to pressure cells at depth, d=5 cm. Results show recovery of initial pressure at each load cycle indicating a possible elastic behavior at the level of soil pressure. Intuitively, the highest increase in pressure (ΔP) of 17 kPa is recorded by pressure cell PC2 in the loading direction followed by pressure cells PC1 (ΔP=15 kPa) and PC3 (ΔP=15 kPa) in directions 1 and 3 respectively. Symmetry in loading and geometry is well captured through the pressure cells PC1 and PC3 and pressure cells PCcentre and PCaxis at the central axis of symmetry. However, the pressure cell in direction 4 possesses a distinctive behavior at a maximum load of 10 kN where a plateau-like shape can be observed contrary to the sharp edges captured by other pressure cells. The possibility of detachment is eliminated as the same sensor was seen to have captured higher pressure values in subsequent tests than the maximum presented in **Fig. 27**.

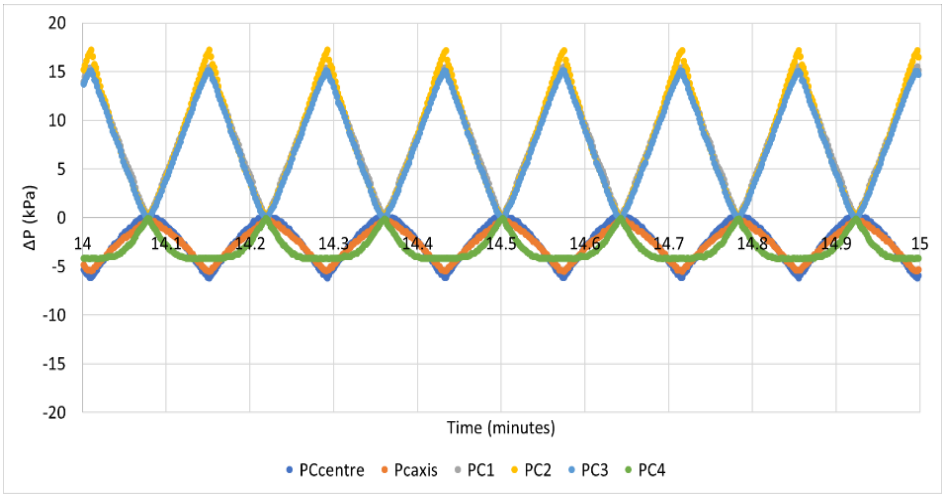

Fig. 27. Pressure measurements below the footing (at d=5 cm) due to cycles of loading of 10 kN force amplitude.

Fig. 28 presents a comparison between the soil distribution at the bottom of the footing in Configuration 1 and that in Configuration 2. While only 3 points are measured, and considered insufficient to draw conclusions, an interpolation of points is made to assume a curve.

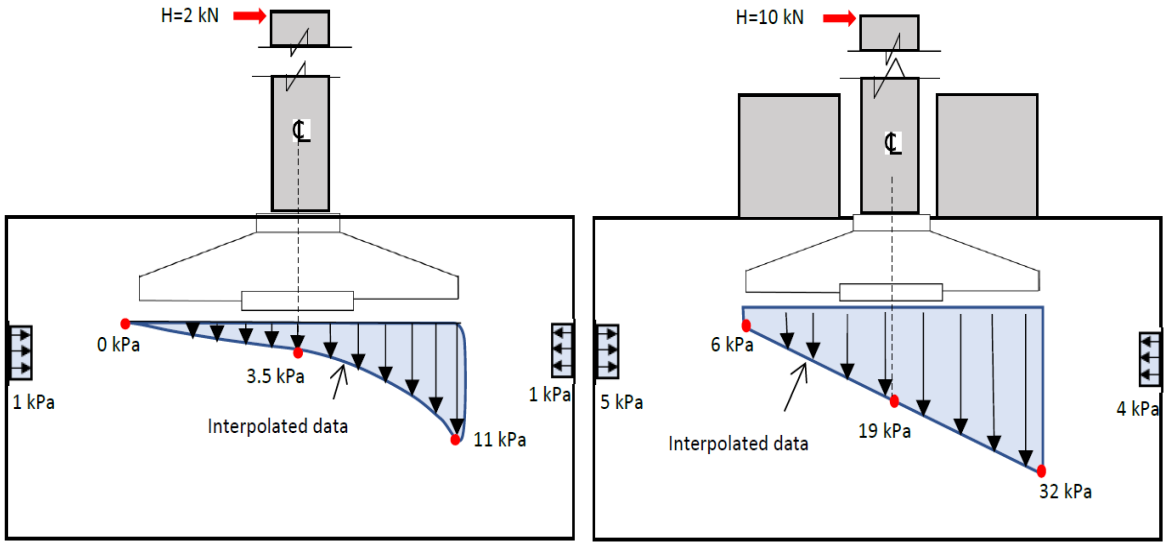

Fig. 28. Pressure measurements below the footing (at d=5 cm) due to total overlying weight and eccentric load; a) Configuration 1 of 2 kN load amplitude and b) Configuration 2 of 10 kN load amplitude.

It can be seen that while configuration 1 offers a concave pressure distribution, configuration 2 tends to produce an approximately linear distribution. The shape of the distribution in configuration 2 is highly influenced by the distribution of the additional loads onto the soil which is largely based on their configuration/positioning.

4.3.2 Failure due to monotonic loading

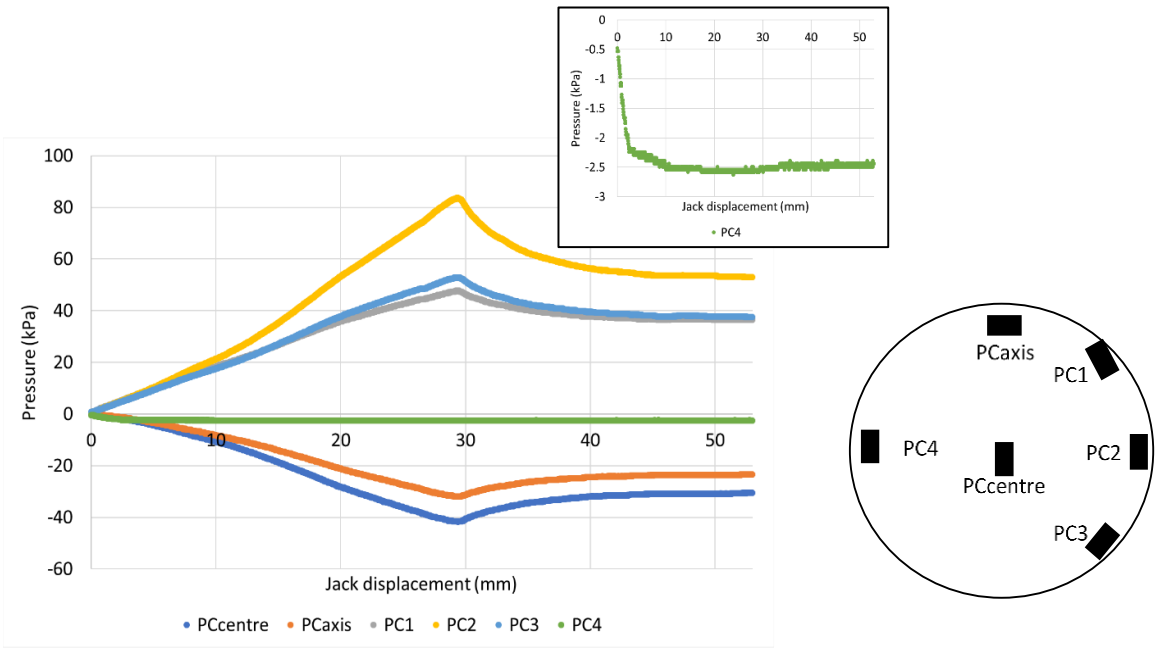

Fig. 29. Pressure cells versus jack displacement measurements during monotonic loading.

Following the application of cycles of loading, monotonic loading was applied until failure was reached. The jack sensor recorded a maximum load of 26 kN before descending to an asymptotic force value of 18 kN where it remained constant with a persistent increase in displacement. The post-peak behavior is similar in all sensor measurements that depict a sharp decrease in response following a gradual decrease up to an asymptotic value where the value remains constant. The non-zero asymptotic

value may be indicative of a permanent event (say deformation). Results are shown in **Fig. 29** and **30** for pressure cells and LVDTs respectively.

The pressure cell in direction 4 (PC4) is seen to measure very low-pressure values which it persisted up to the end of the test. This tendency is yet to be understood considering it persists from the beginning of the test (at lower overturning loads) eliminating the possibility of an uplift. On the other hand, pressure cells PC2 is seen to have undergone a total pressure increase of 83 kPa and at the central axis of the foundation PCcentre and PCaxis experience a total decrease of about 40 kPa and 35 kPa respectively. Following the peak values, a decrease to a persistent 55 kPa, 30 kPa and 22 kPa was recorded by pressure cells PC2, PCcentre and PCaxis respectively.

On the other hand, LVDT measurements indicate non-symmetrical displacements due to the eccentric loading applied (**Fig. 30**). While LVDT2 recorded a downward peak displacement of a mere 0.14 mm, LVDT4 recorded 0.52 mm. Also, LVDT4 presents a decrease in vertical displacement post-peak that is relatively more distinctive than that captured by LVDT2.

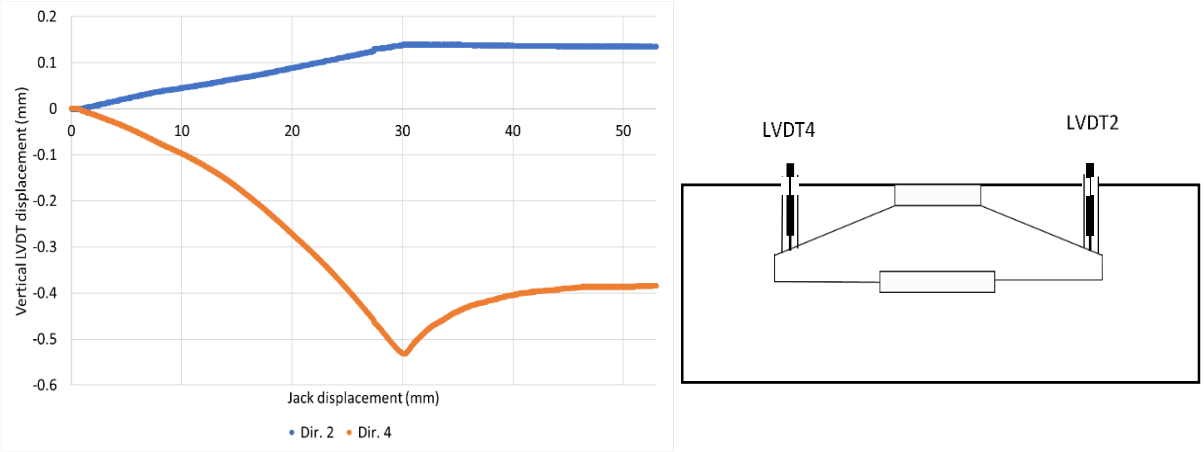

Fig. 30. LVDT measurements on footing versus jack displacement measurements during monotonic loading.

Fig. 31 seeks to determine the differential displacement captured by the LVDTs in the loading direction for the calculation of eccentricity and footing rotation. It can be seen that considering the LVDT measurements at a maximum load of 26 kN, an eccentricity, ‘e’ exists. The formulation is presented below.

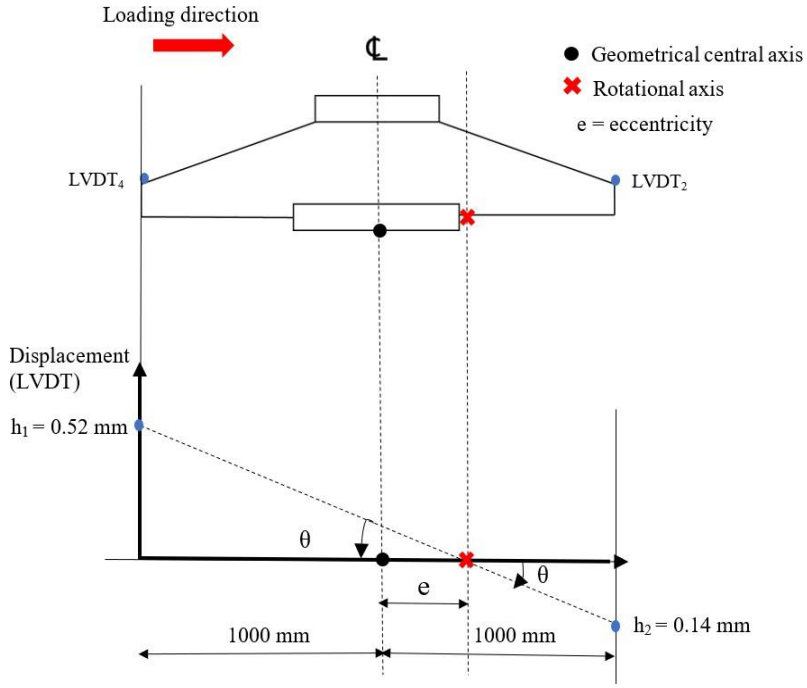

Fig. 31. LVDT measurements at time of maximum load for calculation of eccentricity.

From results of the LVDT measurements, the eccentricity of the loading can be calculated using mathematical laws of similarity as presented in **Fig. 31**. Assuming the LVDTs capture the true rotation of the footing, and that the rotation is that of a rigid body; then the rotation, θ can be determined using Equation 2. Denoting the LVDT2 measurement as h_1, LVDT4 as h_2 and diameter of footing as, D; then the rotation obtained is 0.02°.

$$\theta = \tan^{-1}\left(\frac{h_2 - h_1}{D}\right) = 0.02° \tag{2}$$

From similarity relation,

$$\tan\theta = \frac{h_1}{D/2 + e} \tag{3}$$

Giving eccentricity, e = 0.58 m.

The eccentricity can also be estimated based on the applied moment, *M* and vertical load, *V* as given in Equation 4 and illustrated in **Fig. 32**. For a total load *V* = 170 kN, based on weights of the footing and backfill (~ 20 kN), mast (12 kN) and additional loads (138 kN) and moment, *M*= *H* x *h* where *H*=26 kN and *h*=3.3 m; the eccentricity value produced equals 0.50 m. This value is comparable to that determined by footing rotation from displacement measurements of the LVDT.

$$e = M / V \tag{4}$$

However, based on the formula to calculate the limitation on eccentricity of *e*=*D*/6 used in real footings [23], the limitation on eccentricity is 0.33 m considering the footing diameter equal to 2 m. The resulting eccentricity calculated from the LVDT measurements and moments due to the maximum load of 26 kN produce eccentricity beyond this limitation, which based on the implications of the formula, uplift occurred. However, the limit conditions are used with caution as while it may successfully predict the limits in real shallow footings, it may not be in downscaled models. This is due to reports on erroneous results made upon applying similar design rules for structures of significantly different sizes. Following the sensor results at failure, no visible cracks were observed on the concrete's surface and nor at the footing-mast connection.

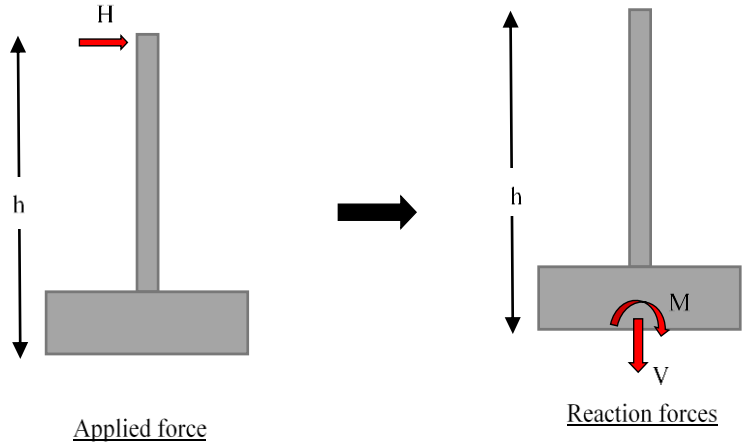

Fig. 32. Resultant moment due to applied eccentric loading.

5 Conclusions

As part of the FEDRE FUI25 project, the current research works have sought to build a stepping stone onto which the reuse of existing onshore wind turbine foundations can be considered through both physical and numerical modeling. The methodology adopted is to allow quantitative comparisons across numerical simulations and sensor measurements in the real scale and laboratory scale; however, only qualitative comparisons are made across the sensors of the two foundation scales. The intention of the current study is to first establish a reliable correlation between experimental and FEM results in the elastic domain before extending the study to nonlinear behavior in future work. Nonlinear effects such

as material yielding, cyclic degradation, and foundation-soil interaction were not modeled but are critical in full-scale scenarios. The following are key findings concerning numerical modeling performed on both scales of the foundations on COMSOL Multiphysics software:

- Results show most critical points due to applied pre-load on reinforced concrete footing and eccentric loading as points near the anchor cage and at top and bottom surfaces of the footing. Fiber optic sensor in the physical model was therefore made to pass through these points.
- Numerical simulations of the small-scale foundation were conducted within the elastic limit through reported similitude relationships. With full downscale of all parameters, similitude in stress and strains is achieved; however, due to practical limitations, only partial similitude was possible. The deviation from a theoretically downscaled wind turbine (a perfect replica of the real structure) was measured through vertical displacements and vertical stress at points in the soil, just below the footing. While the displacement values were seen to deviate from the theoretical model, the stress levels were effectively maintained.
- Numerical simulations were also undertaken to determine the possible effect of two similitude configurations; one without additional loads and another incorporating additional loads. The model without additional loads experienced uplift on the leeward side upon application of the same level of eccentric loading (horizontal load) to obtain same stress levels as those of the real structure. This caused overturning failure to dominate the failure mechanism. However, additional loads eliminated the premature failure of overturning by maintaining the soil pressure at levels similar to that experienced in real conditions.

Since the model is not verified under fatigue or dynamic loading, the primary aim of the 1/10 small-scale model presented in the current study is to determine the load transfer mechanism through a wind turbine system due to quasi-static loading (effect of wind loading only). The following can be concluded concerning the scaled model:

- The sensors were seen to produce values that corresponded quite well with numerical simulations under relatively small applied loads. This gave a good sense of the load transfer from the mast to the underlying soil. Furthermore, symmetry was observed in all sensors positioned at 2 symmetrical sides of the laboratory model. Symmetrical results offered verification to the setup indicating a well centered system rotating about a well-defined axis.
- In the concrete, fiber optic was placed with its coating whose intended measurand was the concrete. Due to its ability to obtain strain measurements along its length, it was found to be most appropriate for comparisons with numerical simulations. At the level of the mast (turbine tower), three displacement techniques were used and produced similar results with errors as low as 0.7% further verifying mast displacements obtained.
- Incorporating additional loads based on similitude relationships can result to soil stress levels similar to those in the referenced real wind turbine system. The additional loads allowed testing of the model up to failure from a monotonic loading that produced a maximum jack force of 26 kN creating a moment at the bottom of the footing of nearly 85.8 kN.m. However, it is only limited to soil-structure interaction problems and not at the level of the concrete footing.

Generally, illustrations are made in the paper on the relevance of physical modeling in understanding the behavior of a complex structure at the scale in which it is modeled. This in turn facilitates improved numerical models based on the adaptation of more appropriate constitutive laws.

Following the results as presented in this paper, two key things can be put into consideration to achieve the ultimate goal of testing the repowering solution.

1) Testing the representativity of the 1/10 scale model under fatigue and dynamic loading. Here, a comparison between the cyclic and dynamic characteristics of the real soil is made to those of the model soil.

2) Measurements of the evolution of material stiffness to quantify the different interaction problems associated with wind turbines.

The model implemented in this study only served the purpose of an initial understanding of the problem; therefore, the repowering solution adopted to the current model will evidently serve the same

purpose.

Future research should incorporate advanced nonlinear modeling to improve predictive accuracy, to capture also reinforcement effects and bond-slip behavior. Scaling limitations pose challenges, but detailed reinforcement modeling and experimental testing beyond the elastic range could enhance FEM-experimental correlation.

Acknowledgement

The authors are in debt to the Technicians of Geotechnics, Materials and Structures Laboratory (GEOMAS Lab), who contributed to the development of the experimental investigation.

Funding Statement

This research was funded by CAPI, BPI France, and FEDER and was enabled through an agreement between a consortium of companies: ANTEA Group, NORDEX, MENARD, CTE wind, PAREX and a research entity INSA Lyon, France, in the framework of the FEDRE project

CRediT authorship contribution statement

J. Modu: Investigation, Formal analysis, Writing – original draft. **L. Brian çon**: Supervision, Investigation, Formal analysis, Writing – review & editing. **J.F. Georgin**: Supervision, Formal analysis. **E. Antoinet**: Supervision.

Conflicts of Interest

The authors declare no conflicts of interest to report regarding the present study.

Data Availability Statement

Some or all data, models, or codes that support the findings of this study are available from the corresponding author upon reasonable request.

References

[1] Connaghan B. Best Practices and Insights: Focus on Partial Repowering. https://www.powermag.com/best-practices-for-wind-project-partial-repowering 2020 (access 01 November 2024)

[2] Haelewyn J, Semete P, Mathieu JP, Escoffier F, Michel-Ponnelle S, Hamon F, Buchoud E. A numerical clone for VeRCoRs mock-up. In: Proceeding of 23ème Congrès Français de Mécanique. Lille, France. 2017. https://hal.science/hal-03465761v1

[3] Bhattacharya S. Physical Modelling of Offshore Wind Turbine Foundations for Technology Readiness Level Studies. Journal of Marine Science and Engineering 2021; 9: https://doi.org/10.3390/jmse9060589

[4] Jalbi S, Arany L, Salem A, Cui L, Bhattacharya S. A method to predict the cyclic loading profiles (one-way or two-way) for monopile supported offshore wind turbines. Mar. Struct. 2019; 63: https://doi.org/10. 1016/j.

[5] marstruc.2018.09.002

[6] Lopez-Querol S, Cui L, Bhattacharya S. Chapter 14 - Numerical Methods for SSI Analysis of Offshore Wind Turbine Foundations, in: Trevor M. Letcher (Eds). A Handbook for Onshore and Offshore Wind Turbines 2017; 275-297: https://doi.org/10.1016/B978-0-12-809451-8.00014-X

[7] Garnier J, Gaudin C, Springman SM, Culligan PJ, Goodings DJ, Konig D, Kutter BL, Phillips R, Randolph MF, Thorel L. Catalogue of scaling laws and similitude questions in geotechnical centrifuge modelling. International Journal of Physical Modeling In Geotech. 2007; 17(3): https://hal.science/hal-00364250

[8] Garnier J. Modèle physique en géotechnique - évolution des techniques expérimentales et des domaines d'application. RFG 2001; 97 : https://doi.org/10.1051/geotech/2001097003

[9] Craig WH. The seven ages of centrifuge modeling. In: Proceedings of the 3rd International Conference on Constitutive and Centrifuge Modelling: Two Extremes. Ascona, Switzerland, 2001: 165-174

[10] Casaburo A, Petrone G, Franco F, De Rosa S. A Review of Similitude Methods for Structural Engineering. Applied Mechanics reviews 2019; 76(6): https://doi.org/10.1115/1.4043787

[11] Kim NS, Lee JH, Chang SP. Equivalent multi-phase similitude law for pseudo-dynamic test on small scale reinforced concrete models, Eng. Struct. 2009; 3: https://doi.org/ 10.1016/j.engstruct.2008.06.008

[12] Lago BD, Flessati L, Marveggio P, Martinelli P, Fraraccio G, di Prisco C. Experimental tests on shallow

foundations of onshore wind turbine towers. Structural Concrete 2022: https://doi.org/10.1002/ suco.20210
[13] 0655
[14] Guo Y, Zhang P, Ding H, Le C. Design and verification of the loading system and boundary conditions for wind turbine foundation model experiment. Renewable Energy 2021; 172: https://doi.org/10.1016/j. renene.
[15] 2021.03.017
[16] Wang H, Liu C, Guo Y, Hao H, Zhang L. Experimental study on the mechanical characteristics of prefabricated dense ribs foundation for onshore wind turbines. Structures 2025; 73: https://doi.org/10.1016/j.
[17] istruc.2025.108273
[18] Bazant ZP, Ozbolt J, Eligehausen R. Fracture size effect: review of evidence for concrete structures. Journal of Structural Engineering 1994; 120(8): https://doi.org/10.1061/(ASCE)0733-9445(1994)120:8(2377)
[19] Picazo Á, Albertini MG, Galvez JC, Vega AC. The Size Effect on Flexural Fracture of Polyolefin Fibre-Reinforced Concrete. Appl. Sci. 2019; 9: https://doi.org/10.3390/app9091762
[20] Knappett J, Reid C, Kinmond S, O'Reilly K. Small-Scale Modeling of Reinforced Concrete Structural Elements for Use in a Geotechnical Centrifuge. J. Struct. Eng. 2011; 137(11): https://doi.org/10.1061/(ASC
[21] E)ST.1943-541X.0000371
[22] Laefer DF, Hong LT, Erkal A, Long JH, Cording EJ. Manufacturing, assembly, and testing of scaled, historic masonry for one-gravity, pseudo-static, soil-structure experiments. Construction and Building Materials 2011; 25(12) : http://dx.doi.org/10.1016/j.conbuildmat.2011.03.066
[23] Lee HS, Woo SW. Seismic performance of a 3-story RC frame in a low seismicity region. Eng. Struct. 2002;
[24] 24 : https://doi.org/10.1016/S0141-0296(01)00135-3
[25] Beguin R, Fry JJ, Picault C, Courivaud JR, Faure YH, Philippe P. Control of the risk of dike failure caused by contact erosion. In: Proceedings of 6th International Conference on Scour and Erosion 2012: 1551-1558
[26] Al Heib M, Emeriault F, Nghiem HL. On the use of 1g physical models for ground movements and soil-structure interaction problems. Journal of Rock Mechanics and Geotechnical Engineering 2020 12(1): https://doi.org/10.1016/j.jrmge.2019.07.006
[27] Basheer IA. Stress–strain behavior of geomaterials in loading reversal simulated by time-delay neural networks. Journal of Materials in Civil Engineering 2002; 14(3): https://doi.org/10.1061/(ASCE)0899-1561(2002)14:3(270)
[28] Surarak C, Likitlersuang S, Wanatowski D, Balasubramaniam A, Oh A, Guan H. Stiffness and strength parameters for hardening soil model of soft and stiff Bangkok clays. Soils and Foundations 2012; 52(4): https://doi.org/10.1016/j.sandf.2012.07.009
[29] Pasten C, Shin H, Santamarina J. Long-term foundation response to repetitive loading. J. Geotech. Geoenviron. Eng. 2014; 140 (4): https://doi.org/10.1061/(ASCE)GT.1943-5606.0001052
[30] Robinson S, Brennan AJ, Brown MJ, Cortis M. Improvement of seabed cable plough tow force prediction models. In: Proceedings of the 8th offshore site investigation and geotechnics international conference (OSIG). London, United Kingdom. 2017
[31] CFMS. Recommandations sur la conception, le calcul, l'exécution et le contrôle des colonnes ballastées sous bâtiments et ouvrages sensibles au tassement. https://www.cfms-sols.org/, 2024 (access 01 November 2024)